KWAJEX

Scientific Overview and Objectives

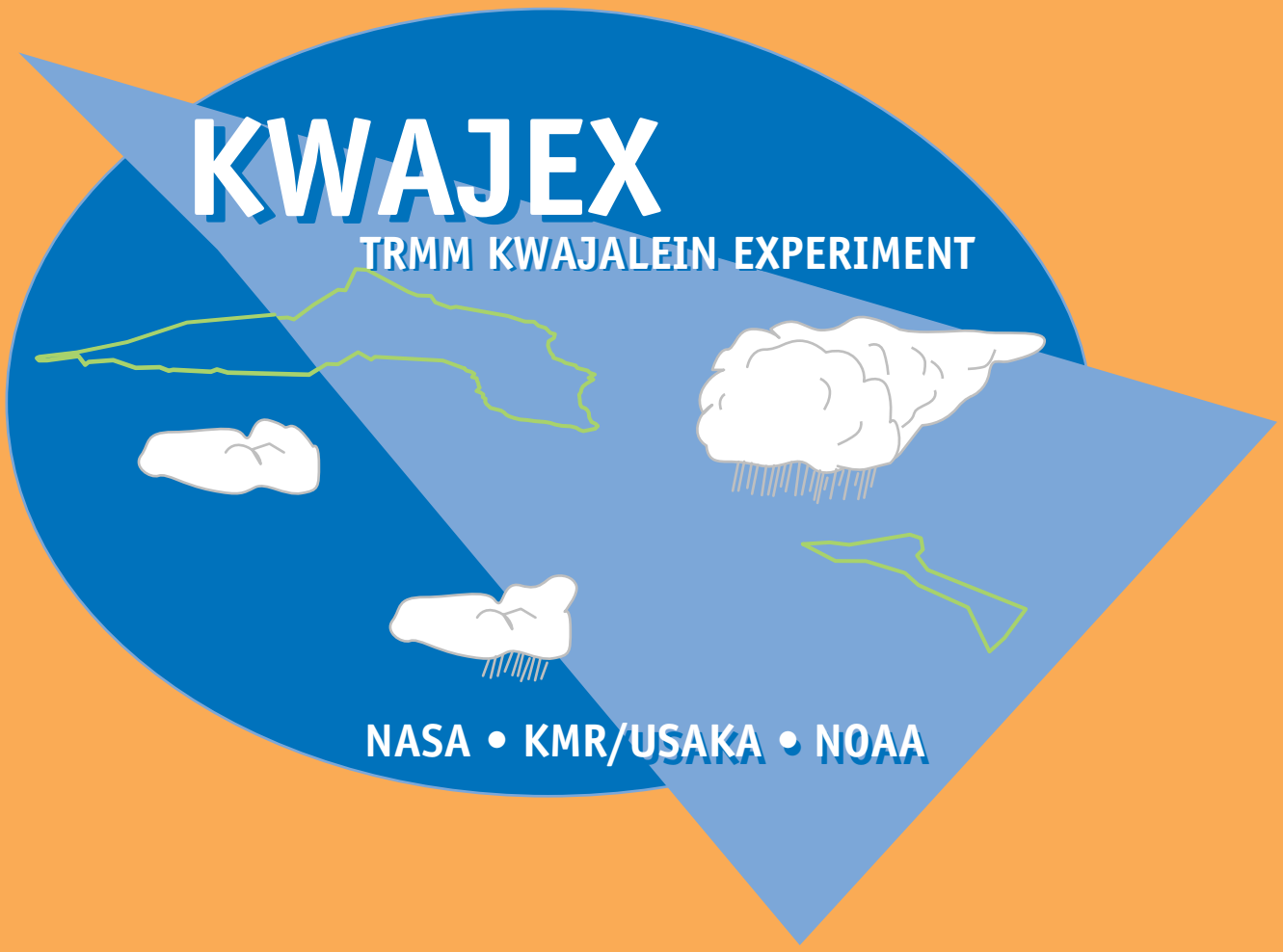

Version
24 February 1999

Table of Contents

Purpose of this document

This document presents an overview of the scientific issues related to the generation of TRMM products over the tropical open ocean and the experimental design for the TRMM field campaign centered at the permanent Ground Validation site on Kwajalein Island in the Republic of the Marshall Islands. The Kwajalein Experiment (KWAJEX) is unique among the planned TRMM field campaigns in that it is the only one to be conducted over the tropical open ocean. While there are similarities in the scientific issues over land and ocean, there are also differences in the issues and their priorities over the ocean. The first part of this document will focus on the scientific priorities related to TRMM products over the tropical open ocean; the second half will describe how these scientific issues will be addressed in the experimental design.

The scientific goal of KWAJEX

The TRMM Level 2 and Level 3 products are designed to yield information needed to calculate the perturbation to the large-scale balanced flow caused by precipitating cloud systems. Global climate models simulate the large-scale balanced flow of the atmosphere. Changes in the large-scale balanced flow with time are described in the tropics by the large-scale vorticity equation. The forcing function for the large-scale vorticity has two terms: one related to the vertical gradient of heating and the other related to momentum transport. The primary goal of TRMM is to address the vertical gradient of heating term and thereby provide observational verification to global models regarding the perturbation of the balanced flow by precipitating systems. In the tropics, the vertical profile of the large-scale horizontal divergence is equivalent to the vertical gradient of heating but is more easily measured. Therefore, the profile of horizontal divergence over a precipitating region is in effect the perturbation caused by precipitation felt by the balanced flow.

The TRMM Microwave Imager (TMI) and Precipitation Radar (PR) will be used as input both separately and combined into algorithms to produce the Level 2 and Level 3 products. The TRMM Ground Validation (GV) data serves as a means of verifying these products over the regions of the GV sites. However, comparison to end products such as surface

rainfall is not sufficient for the purposes of validating and calibrating the satellite data and satellite algorithms since it does not address why the differences exist. Physical validation of the assumptions used in the TMI, PR, and GV algorithms is vital to correcting errors and improving all TRMM algorithms so that they reach the right answers for the right reasons. The GV sites cover only a tiny fraction of the TRMM satellite coverage. The GV data can serve as a check on the satellite algorithms but only over these limited regions. The verification of physical assumptions has impact on the global TRMM products and our confidence in their accuracy both at the GV sites and between them.

Of the routine GV data, the 3-D reflectivities (2A-55, 3A-55) are the only means of accessing the characteristics of the three-dimensional storm structure that are the basis of many of the physical assumptions used in the TRMM satellite algorithms. While useful, these routine 3-D reflectivity data are limited in terms of the types of information they provide and are not sufficient to address many specific aspects of physical validation for TRMM algorithms. The TRMM field campaigns address this deficiency by providing limited time periods of intensive observations at GV sites by multiple specialized sensors and platforms to collect data directly related to physical validation issues that would not be available otherwise. It is important that the field campaigns be designed in a manner such that the benefit for physical validation of *all* algorithms is maximized given the allocated resources. The first part of this document describes the scientific issues and physical validation needs of TRMM algorithms over the tropical open ocean as a background for the second part, which will relate observational needs to specific instruments and platform resources and the deployment of these resources in the KWAJEX field campaign.

PART I: Scientific Overview

1. Scientific issues to be addressed in KWAJEX

1.1 Temporal sampling

Among the stated goals of TRMM is the global mapping of precipitation on monthly time scales and over $5° \times 5°$ areas. The TRMM satellite is in a low earth orbit and observes a given area intermittently. Regions in the higher latitudes of the orbit coverage are observed more frequently than those in the tropics. Errors in the monthly averages will consist of a combination of the errors in the instantaneous retrievals of precipitation and errors associated with intermittent observation. Instantaneous retrieval errors will be addressed in Sections 1.2-1.4. The sampling error is determined by the orbit of the satellite, the swath width scanned by the satellite as it passes over, and the statistical characteristics of the observed rainfall (Bell et al. 1990).

Studies to date of the TRMM sampling errors (Bell et al. 1990; Bell and Kundu 1996) have used the GATE rain map data set as input to mathematical models used to compute the statistical characteristics of the rainfall. Rainfall characteristics that impact sampling error are the diurnal cycle of rainfall, the areal extent and distribution of the precipitating regions, and the lifecycle and duration of regions of rainfall. In order to assess the variation of sampling error in different regions of the globe, research similar to the Bell studies will need to be carried out for other regions such as Kwajalein where precipitation characteristics are different from those in tropical Atlantic Intertropical Convergence Zones near the African coast.

The TRMM GV sites are the logical choice for these future sampling error studies since they are collecting data over the lifetime of the TRMM satellite. During GATE, rain maps were produced at hourly intervals over a region ~131,000 km^2 over ~100 days (Hudlow and Patterson 1979). Given the 150 km radius of the GV 2A-53 rain maps, approximately 4400 GV rain maps (~3 months worth) would be required to produce a rain map database equivalent to that from GATE.

Validation studies of the methods (Bell and Kundu 1996) used to produce monthly products from the intermittent satellite samples will utilize comparisons of monthly average products from the TRMM satellite and GV data. Many months of data will be required to have sufficiently large samples to detect systematic biases and random error. The time scale of the proposed KWAJEX field campaign (2 months) is too short to address temporal sampling issues directly. However, analyzing the GV data in the context of the other observations during the field campaign will improve the physical interpretation of the routine GV data. In this way, the field campaigns at the permanent GV sites will make the routine GV data more valuable and thus contribute to the examination of temporal sampling issues indirectly.

1.2 TRMM microwave imager (TMI)

a. Basic concepts

Satellite passive microwave precipitation estimation techniques utilize the modification of surface upwelling radiation by precipitation. Both scattering and absorption reduce energy reaching the surface. Absorption of incoming energy by intervening materials causes them to emit radiation (through Kirchoff's Law) which increases the upwelling brightness temperatures compared to a situation when no absorbing materials are present. Scattering reduces the upwelling brightness temperature. Water at the earth's surface has low emissivity at microwave frequencies and thus presents a cold background which makes the small increase in brightness temperature associated with absorption by precipitation detectable. Land has larger and variable emissivities and presents a much warmer background against which the absorption signal is difficult to detect unambiguously (Wilheit 1986). Scattering is detectable over both water and land.

Among the atmospheric constituents, only precipitation scatters microwave radiation. The degree of scattering and thus the depression in upwelling brightness temperatures caused by scattering is a function of hydrometeor type and mixing ratio. Liquid water both absorbs and scatters. Ice primarily scatters microwave radiation, though it does absorb to a small degree. The absorption of microwave radiation is expressed by $\sigma_a D$ in which D is the depth of the rain layer and σ_a is the volume absorption coefficient, a function of the mixing ratios of rain,

cloud droplets, and water vapor (Kidder and Vonder Haar 1995). Microwave radiative transfer in a precipitating media is dominated by absorption below 22 GHz and ice scattering above 60 GHz. Between 22 and 60 GHz both scattering and absorption are important and either may dominate depending on the specific situation (Wilheit 1986).

Microwave brightness temperatures (T_b) are thus sensitive to the *column* scattering and absorption properties which in turn are dependent on hydrometeor types and their mixing ratios within the column. The vertical profile of hydrometeors is not linearly related to surface rainfall (Smith et al. 1992; Kummerow 1998, etc.). Current passive microwave precipitation estimation algorithms approach the problem of relating brightness temperatures and surface rainfall by using some combination of "empirical" and "physically based" methodologies (Smith et al.1999). Empirical algorithms derive a statistical regression between measured brightness temperatures at several frequencies and ground measurements of rainfall (radar and/or rain gauge). The TRMM Day 1 passive microwave algorithms use physically based passive microwave rainfall retrieval. Smith et al. (1992) described the conceptual basis for physically based passive microwave rainfall retrieval in their conclusions:

> "These results emphasize that the underlying remote-sensing problem involves the detection of liquid and frozen hydrometeors well above the surface, not the detection of near-surface rain rates. It is through the guidance of a cloud model that this information can be used in a consistent fashion to describe the entire vertical hydrometeor structure. In essence, we contend that the optimal approach to estimating rainfall from passive microwave measurements is to first determine the constituent profile of hydrometeors in the middle and upper reaches of the clouds, that is, in the region of the atmosphere where multifrequency measurements are most sensitive. This profile information can then be used in conjunction with a properly designed cloud-radiation database that contains complete information on the hydrometeor profiles and surface rain rates, involving the inherent intercorrelations of the microphysics from upper to lower atmosphere and avoiding any arbitrary assumptions concerning hydrometeor structures and particle sizes."

A simplified version of how these concepts are implemented in physically based passive-microwave precipitation retrievals such as used in TRMM is as follows (Kummerow 1998): Cloud models are initialized with observed upper-air soundings and other data to produce

realistic simulations of the atmospheric, cloud, and precipitation characteristics of storms. Of the many possible outputs from the cloud model, a subset is further processed for use as input into forward radiative transfer calculations. In particular, regions within the storm simulation with surface rainfall rates within specified intervals and associated with convective and stratiform precipitation types are identified and averages of the vertical profiles of mixing ratios of different hydrometeor types and cloud water are computed over these regions. The forward radiative transfer calculation (Fig. 1) is then made for each rainfall interval/precipitation type using the averaged vertical hydrometeor profiles to produce brightness temperatures at each of the TRMM TMI frequencies. The cloud model and radiative transfer calculations yield sets of brightness temperatures associated with different surface rainfall rates and precipitation types. This information is combined to derive nonlinear analytical expressions relating T_b to surface rainfall rates, for different categories of precipitation type and rain layer thickness.

Our understanding of the sources of error and their magnitudes in the various aspects of physically based passive-microwave precipitation retrievals varies. These sources can be broken into several categories: errors associated with radiative transfer calculation itself, errors associated with inputs to the radiative transfer calculation, and errors associated with use of average characteristics to represent precipitation structure that is horizontally inhomogeneous on the spatial scale of the radiative transfer calculation (beam filling).

b. Errors associated with radiative transfer calculation

For the purposes of this section we will consider errors in the radiative transfer calculation assuming that the input parameters are perfect. These types of errors constitute only a small portion of the overall error in microwave retrievals but will be discussed for completeness. The use of 1-dimensional versus 3-dimensional radiative transfer calculations is the primary focus of research in this area.

By Kirchhoff's Law, absorptivity = emissivity at a particular wavelength. Thus calculating absorption also yields emission. The volume absorption coefficient σ_a is a function of the vertical profile of mixing ratios of rain, cloud droplets, and water vapor. If these are known,

σ_a can be calculated using electromagnetic solutions for the absorptive properties of rain, cloud droplets, and water vapor all of which are fairly well understood (Kidder and Vonder Haar 1995). In contrast, ice scattering is much more difficult to model. Electromagnetic solutions for ice scattering are only available for a few simple shapes such as spheres and ellipsoids; the modeling of more complex shapes such as dendrites, aggregates, rimed ice, and graupel is considered to be intractable (Oguchi 1983; Wilheit 1986). The only means of deriving ice-scattering characteristics for these commonly occurring ice particles is by empirical studies involving cloud physics measurements of ice particle types, crystal habits, and mixing ratios and their associated microwave scattering.

The mixing ratio of water vapor decreases exponentially with height in the atmosphere. Similarly, the concentration of ice above the 0°C level decreases with height as well. Additionally, the nature of ice particles changes with temperature (altitude). The maximum dimension of aggregates tends to increase with increasing temperature (decreasing height) so that the largest aggregates occur between –4 to 0°C (Hobbs et al. 1974). The backscattered cross section of particles increases more than linearly with particle size (e.g., D^6 at radar frequencies). Thus the layers of ice particles with the greatest impact on microwave scattering will be those in regions of higher ice particle concentrations and with larger sizes. These characteristics are maximized in the region just above the 0°C level. High altitude ice with its small size and low number concentration has little to no relevance to microwave radiative transfer calculations (Kummerow, personal communication).

The region just above the 0°C level, which is of vital importance to microwave ice scattering, has a high probability of containing super-cooled water. Super-cooled liquid water drops, when present, are usually found at temperatures between 0 to –20°C with the highest mixing ratios observed close to the 0°C level. Aircraft penetrating these regions will encounter severe icing conditions since supercooled droplets freeze when they collide with an aircraft (Wallace and Hobbs 1977).

The mixed-phase layer (e.g., radar bright band) within a precipitating cloud, where ice melts and particles of pure ice, pure liquid water, and combination ice-water hydrometeors are present simultaneously is very poorly understood. Since this region is too complex to model electromagnetically, the only means of deriving absorption and particularly scattering

properties of the mixed-phase region are simultaneous observation of microwave radiances and in situ cloud physics measurements. The cloud physics measurements must be able to distinguish between ice and water particles within the full spectrum of hydrometeor sizes (0.2 mm - 6+ mm) in order to resolve the respective concentrations of ice versus liquid water scatterers.

c. Errors associated with inputs to the radiative transfer calculation

Most of the inputs to the radiative transfer calculation can be produced by cloud models and thus their accuracy and precision is directly related to how well the cloud model simulates the various fields of the storm. Discussion of cloud model uncertainties is deferred until Section 1.5. However, it is clear that for physically based passive microwave techniques, the better the cloud model works, the better the input to the radiative transfer calculation and thus the better the derived brightness temperature to surface rainfall rate relations.

The calculation of absorption of microwave radiation requires the following primary inputs: the brightness temperature of the surface (which is a function of surface emissivity), surface temperature, and surface roughness, the incoming microwave radiation from the cosmos, the depth D of the rain layer, and σ_a the volume absorption coefficient (which is a function of the mixing ratios of rain, cloud droplets, and water vapor). Surface roughness (a function of surface wind speed) is usually assumed, and all the other parameters are usually derived from the cloud model output (Kummerow 1998). However, as a check of model output it would be useful to observe these inputs directly and use the observations as input to the radiative transfer calculations. Of these inputs, the radiative transfer calculation is particularly sensitive to depth of the rain layer and the vertical profile of hydrometeors from the top of the mixed-phase layer to the surface.

For TRMM satellite data, the presence of the PR instrument permits direct measurement of the depth of the rain layer. Rain depth can also be observed directly by the GV radars. The use of observed rain depth rather than a climatological freezing level will reduce the uncertainty in radiative transfer calculations. The rain depth is not at the climatological 0°C level in the following types of conditions: warm-rain situations where the rain layer does not

extend to the freezing level, where a storm has induced a localized change in 0°C level, and in regions where super-cooled rain is present (Wilheit 1986). With a minimum sensitivity in reflectivity of ~17 dBZ, the PR cannot address the depth of the meaningful ice-water path.

The vertical profile of drop size distribution (and hence rainrate and reflectivity of hydrometeors) from below the mixed-phase layer to the surface is controlled by interrelated factors of horizontal and vertical air motions, nucleation from the vapor phase, condensation, evaporation, collection, drop breakup, and fallout (Houze 1993). Such complex interactions can only be assessed using a cloud model. Surface-based scanning radars are limited in their ability to address this issue because of their coarse vertical resolution (~1-2 km) compared to ground-based and airborne vertically pointing radars (100-500 m resolution). Additionally, the scanning radar beam does not sample to the surface due to curvature of the radar beam away from the surface with increasing range, which is related to both atmospheric refraction and the curvature of the earth. Radar reflectivity cannot be mapped uniquely to drop size distribution. Measurements of radar reflectivity and Doppler velocity along a vertically pointing beam require the use of many assumptions to infer drop size distribution (Wakasugi et al. 1986; Gossard et al. 1990). In order to address the effects of inhomogeneity in the vertical on brightness temperatures, measurements of hydrometeor profiles with very high vertical resolution (ideally < 100 m) are needed.

Although there are uncertainties in ice scattering modeling, studies have shown a strong sensitivity of particularly high-frequency (85 GHz) microwave brightness temperatures to the vertical profile of ice (Adler et al. 1991). Additionally, graupel has been shown to have a dominating attenuating influence on true emission sources due to backscattering (Smith et al. 1992). The presence of and location (above or below the 0°C level) of graupel within a column are thus important parameters in the radiative transfer calculation. In terms of microwave retrievals, it is therefore particularly important to validate the graupel field in cloud models.

The current TRMM TMI algorithm uses different hydrometeor profiles for convective and stratiform precipitation. The cloud-model-produced hydrometeor profiles need to be

verified with observations in terms of their constituents and mixing ratios in *both* convective and stratiform precipitation.

d. Errors associated with horizontal inhomogeneity

Beam filling is a basic characteristic of all electromagnetic sensors. Electromagnetic beams widen as a function of range and beam width; when the beam intersects a particular volume of atmosphere the returned energy is a function of the incident energy and the number, size, and types of scatterers but not the spatial distribution of scatterers within the volume. Two volumes of atmosphere containing the same number of scatterers of the same size and type will scatter the same amount of energy independent of the spatial distributions of the scatterer (Fig. 2). The beam filling "problem" is actually the assumption made for mathematical convenience that the scatterers are uniformly distributed in the volume. The only true solution to beam filling is to use a sensor whose characteristics are such that the spatial scale of the features of interest is similar to or larger than the field of view (FOV) of the beam. Thus using the same algorithm, passive microwave precipitation retrievals are more accurate using the higher resolution TRMM TMI sensor than the coarser-resolution SSM/I sensor (Kummerow, personal communication).

When beam filling cannot be eliminated, then the uncertainties related to the inhomogeneity of the observed field can be quantified with an error model. For passive microwave retrievals, error models relate inhomogeneities in the rain field (i.e., inhomogeneities in the hydrometeor profiles) within the satellite FOV to the brightness temperatures returned from the FOV. The inhomogeneity of the rain field is defined mathematically in terms of the mean variance of the rain field within the satellite FOV, the change in the mean inhomogeneity from one month to the next, and the uncertainty in any given satellite FOV (Kummerow 1998). These statistics are derived from surface-based radars which are capable of providing rainfall data at higher resolution than the satellite FOV. There is a tradeoff between the resolution of input radar data and the amount of available data. Since the radar beam widens with increasing range, choice of a finer resolution decreases the maximum range at which data can be used, reducing the size of the

data set. Kummerow (1998) used 2 km resolution since this resolution corresponded to the analyzed TOGA COARE shipborne rain maps (Short et al. 1997) and the TRMM GV 2A-53 products. Kummerow (1998) used the Goddard Cumulus Ensemble model (Tao and Simpson 1993) to construct mean hydrometeor profiles as functions of surface rainfall. These hydrometeor profiles were used as input in the radiative transfer calculations.

A more direct evaluation of errors associated with horizontal inhomogeneity can be made using observed (rather than modeled) hydrometeor profiles obtained in conjunction with observed microwave radiances. These measurements are needed at 2 km horizontal scale (i.e., half the scale length from the surface to the 0°C level; Wilheit, personal communication). The ensemble of hydrometeor profiles can also be used to characterize the time and spatial scales of the horizontal inhomogeneities in both convective and stratiform precipitation regions.

Kummerow (1998) found that horizontal inhomogeneity of the rain field was a larger source of error than use of one-dimensional versus three-dimensional radiative transfer calculations. He found that the microwave brightness temperature of a homogeneous field is higher than the brightness temperature of an inhomogeneous field with the same rain rate. In addition, *the brightness temperature does not respond to the surface rainfall rate directly but instead responds to the integrated hydrometeor content in the cloud* (Kummerow 1998). In other words, uncertainty in the horizontal rain field is, in the context of passive microwave measurements, the uncertainty in the vertical profile of hydrometeors in space and time. Thus, the horizontal spatial variation of microphysics in the rain region, the ice region, and the mixed-phase region are all important in addressing errors associated with horizontal inhomogeneity.

1.3 Precipitation radar (PR)

The TRMM K_u band Precipitation Radar (PR) is strongly attenuated by rainfall. A potentially large source of error in TRMM PR products is the error associated with the attenuation correction that is applied to the satellite data before it is further processed into reflectivity profiles, convective/stratiform maps, and rain maps.

Several methodologies are commonly used to constrain the total path-integrated attenuation. The first type follows Hitschfield and Bordan (1954) and calculates the attenuation from the top of the rain echo to the surface. Surface reference methods are the second type of attenuation correction; these use the attenuation of the surface echo to estimate the attenuation correction upward through the rain echo. Surface reference methods are sensitive to factors affecting the surface roughness of the ocean such as surface wind and raindrop impact. The Day 1 PR 2A-25 algorithm (PR profile) is a hybrid algorithm using a combination of both top-down and bottom-up techniques to correct the observed reflectivities for attenuation. A third type is the mirror image algorithm (Meneghini and Atlas 1986) which utilizes a combination of direct and mirror-reflected reflectivities to derive the attenuation correction. The mirror-image algorithm is restricted to nadir data and is sensitive to surface roughness. The verification of the attenuation correction schemes requires "true" nonattenuated radar reflectivity data such as from an S-band radar which only become noticeably attenuated in heavy hail or rain mixed with hail (Ryzhkov and Zrnic 1995). Verification is ideally done at the same spatial resolution as the K_u band radar data. However, when this is not possible, comparisons can be made by degrading the K_u band data to the coarser resolution of the S-band data and comparing them at those scales.

Observational needs specific to the PR are nonattenuated reflectivity, to compare to the attenuation-corrected PR data and sea surface roughness. In practice, sea surface roughness is usually crudely estimated as a function of wind speed but the interaction of rain drops with the sea surface at capillary-wave scale is poorly documented (Atlas 1994). Direct observations of sea surface roughness at capillary scale (few cm) are needed as a function of wind speed and rain rate to quantify this parameter. Scientific issues related to the classification of convective and stratiform precipitation and to the mapping of reflectivity to dropsize distribution and rainfall rate are discussed under Ground Validation data in the following sections.

1.4 Ground validation algorithms

The primary goals of routine TRMM ground validation at GV sites such as Kwajalein are to provide convective and stratiform precipitation maps (2A-54), 3-D precipitation structure (2A-55), and rain maps (2A-53). The details of the routine ground validation data sets at Kwajalein and their application in validating TRMM satellite data are discussed in Section 3.2. This section will discuss the scientific issues related to each of these products.

a. Convective/stratiform precipitation

The net heating of the large-scale environment by mesoscale convective systems is dominated by condensation and evaporation associated with vertical air motions. In the diagnostic framework, "measurements" of tropical heating essentially consist of estimates of vertical mass flux, derived in turn from estimates of the horizontal divergence of measured winds (e.g., Yanai et al. 1973). Divergence profiles are integrated vertically to yield vertical velocity and heating profiles.

Houze (1989) discussed two distinct types of heating profiles (Fig. 3) which have been labeled as "convective" and "stratiform" because of their association with convective versus stratiform precipitation and velocity structures. Convective regions have mean vertical motion profiles with mean upward motions at all levels (except sometimes near the surface). The altitude of maximum mean vertical velocity varies in height as the convective region matures, and the altitude of maximum heating follows the vertical velocity peak (Houze 1989; Yuter and Houze 1995). Vertical motions within stratiform regions have a characteristic profile of mean upward motion in the upper troposphere and mean downward motion in the lower troposphere with the level separating the two located near the 0°C level (Houze 1989; Biggerstaff and Houze 1991, 1993; Mapes and Houze 1995; Yuter and Houze 1995). Diagnostic calculations of stratiform vertical motion profiles thus imply heating of the upper troposphere and cooling of the lower troposphere.

Within the TRMM context, the primary purpose of the convective/stratiform maps (both GV and satellite-derived) is to partition the vertically integrated heating (rainfall minus evaporation) by identifying regions characterized by one of the two distinct horizontal

divergence profiles. In the context of TRMM, a "useful" definition of convective versus stratiform precipitation corresponds to precipitating regions that have "convective" versus "stratiform" divergence (and hence heating) profiles.

In physically based passive microwave precipitation retrievals, the convective/stratiform classification has an additional purpose: it is used to account for the fact that different vertical hydrometeor profiles can produce the same surface rainfall. At rainrates < 10 mm/hr, the ensemble characteristics of microphysical data in convective versus stratiform regions in tropical precipitation are a subject of debate (Tokay and Short 1996; Yuter and Houze 1997).

The intrinsic horizontal scale of convective and stratiform precipitation regions is also a subject of debate with some arguing that convective and stratiform characteristics are a result of the ensemble properties of regions of several to tens of km in scale (Churchill and Houze 1984; Steiner et al. 1995; Houze 1997; Yuter and Houze 1997) while others argue that convective and stratiform characteristics can be manifest over regions a few hundred meters in scale or less (Atlas et al. 1995; Tokay and Short 1996). For TRMM TMI, PR, and combined algorithms the convective/stratiform classification is needed at 4 km horizontal scale (Smith and Wilheit, personal communication).

While it is generally agreed that regions with strong updrafts and downdrafts and vertically oriented reflectivity maxima are associated with "convective" divergence profiles and that regions with weak updrafts and downdrafts are associated with "stratiform" divergence profiles, the classification of intermediary or transitional regions whose dynamical and microphysical characteristics are neither clearly stratiform nor convective is a subject of debate.

Data collected in KWAJEX will be used to address the following convective/stratiform algorithm issues in the context of TRMM.

- The 3-D horizontal divergence data derived from dual Doppler radar data (ship radar combined with Kwajalein S-band radar) will be used to improve and verify the convective/stratiform classification of GV radar data with regard to intermediate areas. Convective and stratiform areas will first be identified by the current GV algorithm using

the routine GV low-level reflectivity data as input. The average dual-Doppler horizontal divergence profiles for the convective and stratiform regions would then be computed and examined. The convective/stratiform algorithm will then be modified slightly, rerun, and the average horizontal divergence profiles for the convective and stratiform regions recomputed; an improvement in the algorithm would be defined such that it would produce more pure convective and stratiform horizontal divergence profiles. This iterative process to refine the convective/stratiform algorithm will use a subset (e.g. one half) of the 3-D horizontal divergence fields collected during KWAJEX. The other independent half of the data set could be used to compare the proposed new algorithm to the original algorithm. This methodology of refining the 2A-54 algorithm would have the additional benefit of defining the classification error in terms analogous to the error in identifying regions with different divergence profiles and thus will aid in quantifying the error in a form directly applicable to the vertical gradient of latent heating calculations.

- Once the convective/stratiform classification has been satisfactorily refined, the mapping of microphysical characteristics and vertical hydrometeor profiles into convective and stratiform regions will be objectively examined. The microphysical data collected in regions classified as convective versus stratiform will be compiled and the ensemble characteristics analyzed in terms of joint probability distributions of hydrometeor type and number concentration by altitude (temperature). In this manner, the in situ microphysics data will be used to derive observed vertical hydrometeor profiles in convective and stratiform regions for comparison to model output and for potential use in radiative transfer calculations. Additionally, they will be used to investigate the inverse problem, by first determining statistically distinct groupings of microphysics data in terms of hydrometeor characteristics and then examining how these groupings map into convective and stratiform regions.

b. Precipitation structure

Different storm structures can produce the same surface precipitation. Therefore, validation of satellite-derived rainfall with surface rainfall alone is not sufficient. The TRMM GV 3-D reflectivity product (2A-55) addresses this issue in the routine GV data. From the routine 2A-55 products, it will be possible to determine the variability of the 3-D reflectivity structure within convective, stratiform, and intermediary precipitation areas. However, only with the field campaign data can we address the physical reasons for this observed variability of the 3-D structures. These reasons may be sought via answers to the following questions:

- What is the distribution of 3-D reflectivity structures associated with regions with distinct convective and stratiform divergence profiles?
- What is the distribution of the vertical profiles of hydrometeor types associated with these precipitation structures?
- What is the sequence of dynamical and microphysical processes as convective precipitation evolves into stratiform precipitation?
- What are the initiating mechanisms and how do they affect subsequent growth and organization?

The development of answers to these questions requires information that is not routinely available from the GV data stream: horizontal and vertical winds, in situ cloud microphysics, high temporal resolution atmospheric soundings, and high temporal resolution snapshots of the 3-D structure of microphysics and dynamics within the storm. Flight-level thermodynamic measurements have value in that they are simultaneous with the in situ microphysics and can be used to verify the retrieval of vertical velocities from dual Doppler data. However, in situ thermodynamic measurements along the flight track represent a very small sample of the 3-D volume of the storm and thus are best utilized in the context of 3-D volumetric data collected by other sensors.

c. Hydrometeor mapping

The identification of regions within 3-D volumes containing snow, rain, supercooled liquid water, and graupel is needed to address the temporal and spatial variability of microphysics within precipitating clouds and to understand the mechanisms of storm evolution. Aircraft in situ measurements provide very detailed information about atmospheric conditions, hydrometeor types, and mixing ratios along the flight track. However, the sample along the flight track represents only a tiny fraction of the volume of a precipitating cloud. While in situ data collected during different passes at different altitudes can be extrapolated to characterize larger regions, such extrapolation is subject to potentially large errors.

Ideally, in order to map hydrometeor types in 3-D volumes, 3-D volumetric data are required. Reflectivity data can be used to map regions where echoes do not extend above the 0°C level (e.g. warm rain). Polarization diverse data—Z_{DR} and K_{DP} (specific differential propagation phase) in combination with radar reflectivity can be processed to identify ice-phase and mixed hydrometeor types. These polarimetric data are routinely available at the TRMM GV sites at Darwin and Kwajalein. Of particular importance to TRMM microwave and cloud modeling objectives is the mapping of regions containing graupel. K_{DP} is not sensitive to graupel; however, the combination of Z and K_{DP} can be used to map graupel, graupel/rain, and graupel/snow mixtures within the three-dimensional volume scanned by the radar. Techniques to derive hydrometeor mappings from polarimetric data are being developed using C-Pol data from McTEX and have shown considerable promise (Keenan, personal communication; Zeng, personal communication). In situ microphysics data (which was not available in McTEX) are needed to calibrate these hydrometeor mappings for the Kwajalein region. Once the hydrometeor-mapping algorithms are calibrated, the polarization diverse data from Kwajalein can be used to derive robust 3-D hydrometeor classifications of both the S-band radar volumetric data collected during KWAJEX and the routine GV volumetric data.

The use of aircraft in situ microphysics data to calibrate the radar-based identification of regions containing snow, rain, supercooled liquid water, and graupel is an example of using physical validation data from the field campaign to improve interpretation of routine GV data. The radar-derived hydrometeor fields from the routine polarimetric GV data will thus

make possible a means of *routine* physical validation of TRMM satellite algorithms during Kwajalein overpasses.

d. Surface precipitation estimation

Waldvogel (1974) showed that different drop-size distributions (DSDs) produced from different precipitation structures can yield the same rainfall rate at the surface. If one has measured the DSD in a volume of atmosphere one can calculate radar reflectivity (Z) and rainfall rate (R) directly:

$$Z = \int_0^\infty D^6 N(D) dD$$

$$R = \frac{\pi\rho}{6} \int_0^\infty V(D) D^3 N(D) dD$$

where $N(D)$ is the particle size distribution function such that $N(D)dD$ is the number of particles of diameter D to $D + dD$ per unit volume of air, $V(D)$ is the fall speed of a drop with diameter D and ρ is the density of liquid water.

Ideally, one would therefore measure DSDs directly in 3-D volumes of atmosphere and calculate rain rate (R). Since different Zs associated with different drop size distributions can yield the same R, any derivation of a one-to-one mapping of Z into R must make some assumptions regarding the nature of the drop size distribution.

Use of multiple Z-R relations to generate TRMM rainfall maps (2A-53) begs the question of whether it is practical to distinguish regions with different DSDs using routine GV data (i.e., radar reflectivity only). Yuter and Houze (1997) found that fall streaks which are a ubiquitous feature of regions with radar-observed bright bands (providing one has data of sufficient resolution to resolve them) are associated with different drop size distributions than the precipitation between the fall streaks. Although definitions of stratiform precipitation vary, it is generally agreed that regions exhibiting a radar bright band are stratiform. Horizontal divergence data and in situ microphysics data collected during

KWAJEX will aid in resolving whether the convective/stratiform classification is a practical means of identifying regions with different DSDs (Section 1.4a).

Even if the *Z*-*R* relation is appropriate, use of observed radar reflectivity to derive rainfall is prone to errors associated with horizontal inhomogeneity of the hydrometeor field on spatial scales smaller than the resolution volume (Section 1.2d), and differences owing to attenuation between the measured reflectivity and the true reflectivity of the precipitation particles (Section 1.3). Another source of error in radar-derived rain maps is the modification of the rainfall from below the lowest level radar beam to the surface (Section 1.2c).

The multiple polarization variables such as Z_{DR}, available at the TRMM GV sites at Darwin and Kwajalein, permit us to examine the question of whether regions with different DSDs can be identified with radar data. Z_{DR} is related to the median diameter of the drop size distribution. The polarization diverse variable K_{DP} permits estimation of rainfall without needing to know the DSD since K_{DP} is related to the liquid water content directly and is independent of drop-size distribution in the Rayleigh regime (Sachidananda and Zrnic 1987; Keenan et al. 1999). The signal in both Z_{DR} and K_{DP} is strongest for oblate liquid water drops (> 1.3 mm diameter). Thus neither Z_{DR} nor K_{DP} can distinguish between weak rain rates when the drops are smaller than 1.3 mm and spherical. It is generally agreed that a hybrid algorithm utilizing some combination of observed radar reflectivity, Z_{DR}, and K_{DP} will be needed to map the full range of observed rainrates (Illingworth, personal communication; Wilson, personal communication; Zrnic, personal communication). It is therefore likely that the TRMM GV Day 2 algorithm at GV sites with polarization radars will use some combination of *Z*, Z_{DR}, and K_{DP}.

1.5 Cloud modeling

Cloud modeling is the lynch pin of TRMM. Since neither horizontal nor vertical winds are routinely measured at the GV sites nor by the TRMM satellite, modeling is the primary means by which the vertical gradient of latent heating can be determined routinely from TRMM observations. Additionally, cloud models play a key role in physically based passive microwave retrievals by producing physically consistent hydrometeor, temperature, moisture,

and vertical velocity profiles that are used as input to radiative transfer calculations (Section 1.2c).

A standard approach to improving cloud models is to simulate well-documented cases of storms using observed environmental characteristics (esp. upper-air soundings) to initialize the model. Model outputs are then compared to in-storm observed fields such as microphysical fields derived from aircraft and radar data, and three-dimensional wind fields derived from dual-Doppler radar data. The sensitivity of the model to changes in the nature, temporal, and spatial resolution of its inputs is assessed by varying these inputs and turning on and off various model physical processes. Specific observational data needs for cloud modeling fall into two main categories: those related to initialization and those related to validation.

a. Initialization

The primary data used to initialize cloud models are upper-air soundings (i.e., pressure, temperature, RH, and winds) from the surface to across the tropopause and into the lower stratosphere. Soundings are needed at different locations in the simulation domain and at high time resolution (3 hrly) in order to characterize the horizontal and temporal variation of environmental characteristics. Frequent profiles in the lower stratosphere are needed to resolve gravity waves which modulate convection. Cloud models can be embedded within mesoscale models as a means of insuring boundary conditions physically consistent with large-scale circulations. Mesoscale models are initialized with upper-air sounding data several hundred km upstream and downstream of the cloud model domain.

The Goddard Cumulus Ensemble Model has a strong sensitivity to the input moisture fields from the surface to the tropopause and particularly in the boundary layer (Ferrier, personal communication). High time resolution observations of the variation of low level moisture in the context of the tropospheric variation of moisture are not available from previous field studies. The variation of the low level moisture field over area and time needs to be documented observationally and assimilated as input into the model.

b. Validation

Validation of model-calculated hydrometeor types and mixing ratios, temperature, moisture, and vertical velocity profiles demand aircraft and dual-Doppler data. These observational data serve a dual purpose by both aiding in refinement of the cloud models and in quantitatively assessing the uncertainties of the model output. For TRMM algorithm purposes, validation of the spatial scales associated with distinct profiles is also particularly important (Wilheit, personal communication).

The TRMM passive microwave precipitation retrievals are dependent on the quality of the cloud model microphysics. Within the context of a particular set of air motions, cloud models keep track of the mixing ratios of up to 8 water substance categories: water vapor, cloud liquid water, drizzle, rainwater, cloud ice, snow, graupel, and hail (Houze 1993). The calculation of the interactions among water substance categories is computationally intensive, particularly when the categories are further broken down into size distributions. The complex nature of cloud microphysical calculations makes validation with observed microphysics the only means to document and diagnose errors in the cloud microphysics. To be most useful, the microphysical validation needs to produce data that can be readily compared to model output: mixing ratios and number concentrations of water substance in as many different forms as possible and simultaneous measurements of liquid water content and supersaturation with respect to water and ice as appropriate.

Cloud and mesoscale models tend to overpredict graupel amounts and distribution. Under some conditions, cloud models have indicated graupel within stratiform regions, an apparent contradiction since measurements of ice microphysics within tropical stratiform regions have not indicated any graupel (Houze and Churchill 1987). The detection of graupel above and below the freezing level is thus a priority within both the convective and stratiform regions.

While cloud models often indicate the presence of super-cooled liquid water above the 0°C level in stratiform regions, in situ measurements within tropical clouds have indicated the virtual absence of liquid water above this level (Houze and Churchill 1987). In situ microphysics measurements just above the 0°C level are needed to resolve this issue. Below the 0°C level, the mixing ratio of liquid water and drop size distributions of rain are needed

as a function of height to assess the modification of DSD by evaporation from below the mixed-phase layer to the surface.

To address model validation issues related to storm evolution, the joint variation of the 3-D vertical velocity and water substance mixing ratios are needed at high time (~5 min) and spatial resolution (~500 m in both the vertical and horizontal). Since convective cells have an individual life time of approximately 30 min, aircraft would have to make several passes through a cell within 30 min. Previous in situ microphysical measurements of tropical convective clouds indicate high concentrations of small particles in convective updrafts (Gamache 1990). The measurement of ice particles versus liquid water drop concentrations requires cloud physics measurements that can distinguish between small drops and small ice.

Stratiform regions are longer lived and considered to be more steady state than convective cells. Within stratiform regions, temperature resolution (vertical resolution) is the driving factor. Measurements are needed every 5 to 10 degrees from 0°C to –50°C and at a lower temperature resolution up to the tropopause (–80°C). The regions below the -25°C level contain the majority of the mass of ice particles within tropical storms (Houze and Churchill 1987). Regions with more ice would need to be sampled more frequently than regions with sparse ice since the interactions of ice with the model physics will be proportionally larger where more ice is present.

1.6 Budget studies

The calculation of the apparent heat source (Q_1) and apparent moisture sink (Q_2) in budget studies (e.g. Lin and Johnson 1996) provide an independent means of validating areal surface precipitation estimates of TRMM satellite algorithms. Budget studies for KWAJEX are extremely important for validation of TRMM TMI and combined algorithms applied to both TRMM satellite overpass and TRMM-satellite-like overpass data obtained with the DC-8 aircraft. For TRMM purposes, these types of budget studies will require 3-hourly upper-air sounding profiles within a closed array, and estimates of surface evaporation derived from SST skin temperature and surface winds. The dimension of the closed sounding array should be 50 km or more along each side (Greco et al. 1994). The region within the array should be

observed by radar so that the budget-study-derived precipitation estimate can be further constrained by radar-derived precipitation estimates and horizontal divergence profiles obtained from dual-Doppler radar data.

2. Observational requirements

2.1 Summary of scientific objectives by section

The observation requirements for KWAJEX are summarized from the previous sections in Table 1.

2.2 Hydrometeor sampling

The requirements for sampling in situ microphysics measurements are a function of altitude. Since the vertical mass transport (and hence amount of water condensed) by air motion of a given vertical velocity decreases exponentially with height, most of the water falling as precipitation and absorbing and scattering microwave radiation is in the low-to-mid troposphere. To determine whether models are properly distinguishing liquid and ice phase hydrometeors and correctly representing their mixing ratios for input in radiative transfer calculations, the KWAJEX observations need to emphasize the vertical distribution of hydrometeors in the low-to-mid troposphere.

In situ microphysical observations have indicated that once glaciation occurs, the ice particle concentration within clouds is not sensitive to further lowering of temperature despite the fact that the number of potential ice nuclei increases with decreasing temperature (Fig. 2-34 in Pruppacher and Klett 1978). The causes of rapid glaciation and production of large numbers of ice particles compared to the number of ice nuclei are attributed to ice-multiplication mechanisms (Hallett and Mossop 1974; Hobbs and Rangno 1985). Because of the lack of documentation of the relative amounts of liquid and ice in the lower portions of precipitating clouds, models have great difficulty accurately representing the distribution of liquid and ice hydrometeors in the low-to-mid levels of clouds where the concentration of hydrometeor mass is greater and particle sizes are larger (Hobbs et al. 1974).

The relative priorities of microphysical measurements with altitude as related to TMI, PR, GV, and cloud modeling are summarized in Fig. 4. For microwave and PR objectives, the

highest priority measurements are in the rain region, the mixed-phase region, and the portion of the ice region with the largest size and largest concentration of scatterers (temperatures higher than –10°C). Interest is moderate in the region between –10°C and –25°C and then decreases for temperatures less than –25°C where the mass concentration is lower. Ground validation objectives have high interest in microphysics from the surface to –25°C especially in the first 2 km above the 0°C level where particles aggregate before falling through the melting layer. At altitudes above –25°C, particle concentrations are lower and interest is moderate. Cloud models need validation of water substance mixing ratios throughout the depth of the storm but especially where water and ice (and hence effects of latent heating and cooling) are concentrated below –25°C. Radar echo tops for the taller Kwajalein precipitating clouds are at ~13 km altitude (–65°C); stratiform regions have echo tops of ~11 km (–45°C); and the tropopause is near 15 km (–80°C). The combined interest of TMI, PR, GV, and cloud modeling in microphysical samples as a function of height is summarized in Fig. 5 by weighting interest level as 1 for low, 2 for moderate, and 3 for high and then summing for each of the four scientific facets. Interest in microphysical samples has the strongest overlap below the –10°C level, and decreases slightly between –10°C and –25°C. At altitudes above –25°C, combined interest is about half what it is in the rain layer.

2.3 Needs for simultaneous measurements

The TRMM satellite provides simultaneous microwave and PR measurements. At the latitude of Kwajalein, the satellite overflies the GV site with significant overlap between the satellite swath and GV region only about 15 times per month. To supplement simultaneous data collected during satellite overpasses, simulated overpasses within the GV region will need to be made with TRMM TMI-like and PR-like instruments mounted on aircraft. Since TRMM algorithms are designed to use these data together, it is of benefit that the microwave and PR measurements be as simultaneous as possible in the sense that the measurements are obtained from the same volume of atmosphere at the same time. The easiest way to insure simultaneity is to mount the instruments on the same aircraft. In this way all the microwave and PR measurements will be coordinated. If the microwave and PR instruments are

mounted on separate aircraft then simultaneous measurements will only be available when the flight tracks of the two aircraft are precisely coordinated.

The complexity of the precipitating clouds makes unambiguous interpretation of any single observed variable difficult without other information to put it into context. Thus, when feasible, simultaneous measurements of different variables by the same platform and by different platforms are not only preferable over measurements without other observational context but essential. As a minimum, the scanning S-band radar on Kwajalein Island can provide contextual information in terms of the routine GV products for observations made within 150 km of its location. One of the goals of KWAJEX is to enhance physical interpretation of the routine GV data that will be a primary source of the large data samples required by temporal sampling studies (Section 1.1). KWAJEX data collection by mobile platforms such as ships and aircraft will have its largest impact on the scientific objectives when it is collected within a 150 km radius from Kwajalein island.

2.4 Tradeoffs

Some types of data collection are mutually exclusive of others. Several of the basic types of tradeoffs facing KWAJEX are:

- Use of a scanning radar in volume sector mode, necessary to obtain high time resolution samples, precludes its use for scanning 360° volumes. Thus, if the Kwajalein Island S-band radar is used in sector mode for extended periods of time, the routine GV products (which require 360° scans) for the months of the field campaign will be compromised and not able to be used as input to temporal sampling studies.

- The resolution of dual Doppler data is related to the distance between the two radars (baseline). The shorter the baseline, the higher the resolution. However, the area covered by dual Doppler measurements is related in the inverse manner: the shorter the baseline, the smaller the area sampled and thus the smaller the sample size.

- Slower aircraft speeds are preferable for high quality microphysical sampling but higher speeds will sample longer along-track distances at lower quality.

- Exact simultaneous measurements collected by two aircraft at different altitudes are difficult to obtain particularly if there is a mismatch in speed of the aircraft. Additionally, the presence of one aircraft in the sampling volume of an instrument on the other aircraft can compromise the measurements (e.g. skin painting of aircraft by radar).

3. Kwajalein Overview

3.1 Geography

The Marshall Islands lie in the tropical central Pacific over 3000 km to the southwest of Hawaii (Fig. 6). Most of the Marshall Islands are small in area and form part of coral atolls. Within the Marshall Islands there are two main island chains. Majuro, the capital of the Republic of the Marshall Islands (RMI), is within the Ratak Chain. Kwajalein Atoll is 427 km to the northwest of Majuro and is part of the Ralik Chain (Fig. 7).

Much of Kwajalein Atoll is leased to the United States Army as part of the US Army Kwajalein Atoll/Kwajalein Missile Range (USAKA/KMR). Civilian access to KMR is tightly controlled since living space and water are limited resources on these small islands. The main KMR facilities are on Kwajalein Island on the southern tip of the atoll and Roi Namur Island 78 km to the north on the northern tip of the atoll (Fig. 8). Both these islands have airstrips for fixed-wing aircraft and the facilities on Kwajalein Island are sufficient for jet aircraft. KMR is the point of contact for facilities and resources on the islands leased to the Army. Aeromet Inc. is the meteorological contractor for KMR and operates the weather-related facilities such as the S-band radar on Kwajalein Island, the upper-air sounding facilities on Kwajalein and Roi Namur, and a surface mesonet with stations on several islands. Placement of KWAJEX facilities within KMR jurisdiction requires the agreement and cooperation of KMR and Aeromet.

The US National Weather Service has a cooperative agreement with RMI and administers weather-related facilities such as upper-air soundings and rain gauges within RMI that are not under the jurisdiction of KMR. Placement of facilities on islands outside KMR jurisdiction requires local cooperation which is complex and difficult to obtain. For KWAJEX, these requests would be negotiated through the NWS office in Honolulu.

3.2 Routinely collected TRMM GV data

Through the efforts of the TRMM Office, the S-band radar on Kwajalein Island was upgraded for use as a TRMM GV site. These upgrades included a new antenna (8.23 m diameter), processor, and the addition in March 1998 of dual-polarization capability. The S-band radar at Kwajalein has a sufficiently long wavelength (10.7 cm) so that attenuation by tropical precipitation is minimal and scatterers less than ~6.25 mm in diameter are within the Rayleigh scattering regime. The KMR requirements from this radar are surveillance scans every ~10 min. Between the surveillance scans, the radar can be used in a manner suited to TRMM needs. Thus, unlike the NEXRAD radars at the GV sites in Florida and Texas, the scan strategy of the S-band radar at Kwajalein has been optimized for TRMM GV requirements.

The routine GV Kwajalein scan strategy consists of a surveillance scan (Fig. 9) interspersed with a set of three 360° volumes repeated every 30 min (Table 2). The first volume provides reflectivity and radial velocity data and consists of 22 elevation angles scanned at ~18 deg/sec (Fig. 10). Dual polarization data requires samples in both horizontal and vertical polarizations. The current transmitter/receiver system on the Kwajalein radar is such that sufficient samples at both polarizations can only be collected if the scan rate is slowed to ~8 deg/sec or less. The second and third volumes are scanned at this slow rate and are 11 tilts each (Figs. 11 and 12). These scans provide dual polarization data— Z_{DR} and PHIDP (Φ_{DP}, total differential phase) as well as reflectivity and radial velocity. The vertical resolution of the second and third volumes is similar to that of NEXRAD data; the resolution of the 22 tilt volume is better. The scans for the second and third volumes are interleaved and the data can be combined into higher resolution volumes for statistical analysis.

Data from all three volumes are processed to produce the standard TRMM GV radar products: 1C-51 (Quality Controlled Radar Volume Scans from Ground Validation Sites), 2A-52 (Existence), 2A-53 (Radar Site Rain Map), 2A-54 (Radar Site Convective/Stratiform Map), 2A-55 (Radar Site 3-D Reflectivities), 3A-53 (5-day Radar Site Rain Map), 3A-54 (Monthly Radar Site Rain Map), and 3A-55 (Monthly 3-D Structure). The dual polarization data are not part of the Day 1 TRMM products but are available in 1C-51 form as input to Day 2 algorithm development for rainfall mapping and for research into hydrometeor typing.

The TRMM Office was also instrumental in upgrading the rain gauge network in the vicinity of Kwajalein and facilitating regular data collection from these gauges. Data is regularly received from 12 tipping bucket gauges within two networks. Gauges on islands within KMR jurisdiction are administered by Aeromet Inc. Gauges on other islands are administered by RMI and their data are collected by the NWS office in Majuro. While ten of these rain gauges are within 150 km of the Kwajalein S-band radar, two gauges are within 15 km range and radar data directly over their location is subject to contamination from ground clutter. Thus Kwajalein has 8 gauges within the region covered by the TRMM GV products from 15 km to 150 km range of the radar (Fig. 13).

3.3 Kwajalein climatology

a. Annual

Kwajalein has a typical tropical oceanic climate. The mean daily temperature at Kwajalein is relatively steady at 82°F all year long with highs near 87°F and lows near 77°F. Relative humidity is highest at 06 Local Time (79-85%) and lowest at 12 Local Time (69-77%). On average, the monthly rainfall generally increases from May to October and is lowest in February (Fig. 14a). Surface mean winds are easterly throughout the year. Mean wind speeds are near 4-5 m/s through July-October and increase to 6-7 m/s during December-May (Fig. 14b). The highest winds measured at Kwajalein are associated with tropical storms. On average, tropical storms cross Kwajalein once every 5 years. The months with the lowest tropical storm frequency (0.01) are June-October. The months of November-April have two

to three times the frequency of tropical storms as the rest of the year. Kwajalein averages 9.7 days a year with thunderstorms (lightning), slightly less than Zipser's (1994) estimate of one thunderstorm per month for tropical oceanic precipitation.

Yearly average precipitation exhibits a strong meridional gradient across Kwajalein Atoll with Roi Namur to the north receiving only roughly 60% of the precipitation of Kwajalein Island to the south. The monthly precipitation accumulation map for August 1998 illustrates this basic pattern (Fig. 15). The broadest region of precipitation in the vicinity of Kwajalein and the smoothest gradient of rainfall across the atoll occurs in September and October according to precipitation estimates derived from SSM/I data (Fig. 16).

The ENSO warm event of 1997 contributed to drought conditions in the Kwajalein area during late 1997 and 1998. Figure 17 shows the rainfall recorded at Kwajalein Island during 1997 and 1998. The TRMM satellite and GV radar data sets for August-September 1998 represent conditions during drought recovery and are likely less representative of conditions to be expected during the KWAJEX project period in 1999 than the data obtained during 1997.

b. Radar climatology

Since the purpose of KWAJEX is to provide physical validation for NASA's Tropical Rainfall Measuring Mission, the experimental objectives all revolve around precipitating systems. KWAJEX operations will be focused on the 150 km radius area centered on the Kwajalein S-band radar at 8.72°N, 167.73°E, the TRMM Ground Validation region for Kwajalein. To help develop KWAJEX experimental plans for radar and aircraft and to improve basic understanding of weather conditions in the Kwajalein region, available Kwajalein S-band radar data from July, August, and September 1997 and August and September 1998 have been examined to derive a radar climatology.

For a variety of reasons, the exact calibration of the Kwajalein radar was not determined for the data collected in the summer of 1997 prior to the TRMM satellite launch in November 1997. In order to utilize data from both 1997 and 1998, statistics that are less sensitive to calibration error are examined. A simple metric of precipitation is the area of

echo larger than a particular dBZ threshold. A few dB variations do not change areal statistics based on dBZ threshold significantly but can have a major impact on areal average rainrates particularly at higher reflectivities. For our purposes in this chapter, we will use radar echoes > 20 dBZ to indicate precipitating areas. Keeping the uncertainties in calibration in mind, 20 dBZ corresponds to a rain rate of ~0.4 mm/hr based on the nominal Kwajalein *Z*-*R* derived from historical data.

Variation of precipitating area

The fraction of the 150 km radius GV region centered on Kwajalein covered by precipitating echo is presented as a time series in Fig. 18, histograms in Fig. 19, and as a cumulative plot in Fig. 20. The contrast between the time series for August 1997 and August 1998 and between September 1997 and September 1998 reveals suppression of convective activity during the summer of 1998 associated with the waning influence of the ENSO warm event. Of the months examined, August 1997 was by far the most active. Seventeen rain periods with cumulative echo instantanously covering more than 20% of the GV area occurred in August 1997 compared to roughly 8 periods in September 1997, 2 in August 1998, and 1 in September 1998. In both years, the rain often occurred at 2-3 day intervals. This time scale is likely related to the passage of easterly waves (Reed and Recker 1971). As is common throughout the world, large areally extensive precipitating regions hundreds of km in scale occur much less frequently than smaller, less organized precipitation (Fig. 19). The cumulative frequency plots show that fractional precipitation coverage < 5% of the GV area occurred 60% of the time during summer 1997 and 75% of the time in summer 1998. In constrast, fractional coverage over 20% of the GV area occurred 11% of the time in summer 1998 and only 2% of the time in summer 1997. It is fortunate that KWAJEX did not take place in 1998.

Diurnal cycle

The diurnal cycle of areal fraction of precipitation is relatively weak during the summer, varying less than 50% from the monthly hourly maximum to hourly minimum (Fig. 21). The

lack of consistency between the diurnal cycles in the 1997 and 1998 data makes generalization difficult. During the month of August there is a tendency to favor convective activity from 1200 - 1900 local time and disfavor it in the early morning. During September, the lull in convective activity is later in the day, centered roughly at midday.

Storm morphology

Storms during September 1997 advected across the GV region from the north, northeast, northwest, west, and east. Since surface meteorological time series and upper-air data for this period is not available at this time, it is difficult to assess if the prevailing winds shifted with storm passage or if storm motion was sometimes counter to the low-level prevailing wind.

Precipitation patterns during September 1997 were often chaotic. Three main categories of precipitation patterns observed during this period are illustrated by the examples in Fig. 224a-k:

- large precipitation regions with well-defined, narrow (10-20 km) convective bands and extensive areas of mature convection.
- narrow convective bands 10-20 km in width and 100 km or more in length without associated mature convective regions.
- regions containing less organized convective activity with precipitating regions up to ~20 km in dimension.

The sampling of these distinct precipitation structures will require different aircraft flight track patterns. Part II of this document, the KWAJEX Experimental Plan, will address the specific plans for ground-based, ocean-surface, and aircraft sensor deployment and coordination to accomplish the observational requirements derived from the scientific objectives in Part I.

References

Adler, R. F., H.-Y. M. Yeh, N. Prasad, W.-K. Tao, and J. Simpson, 1991: Microwave simulation of a tropical rainfall system with a three-dimensional cloud model. *J. Appl. Meteor.*, **30**, 924-953.

Atlas, D., 1994: Footprints of storms on the sea: A view from spaceborne synthetic aperature radar. *J. Geophy. Res.*, **99**, 7961-7969.

Atlas, D., P. Willis, and F. Marks, 1995: The effects of convective updrafts and downdrafts on reflectivity rain rate relations and water budgets. Preprints*, 27th Conf. on Radar Meteor.*, Vail, CO, Amer. Meteor. Soc., 19-20.

Bell, T. L., A. Abdullah, R. L. Martin, and G. R. North, 1990: Sampling errors for satellite-derived tropical rainfall: Monte Carlo study using a space-time stochastic model. *J. Geophys. Res.*, **95**, 2195-2205.

Bell, T. L., and P. K. Kundu, 1996: A study of the sampling error in satellite rainfall estimates using optimal averaging of data and a stochastic model. *J. Climate*, **9**, 1251-1268.

Biggerstaff, M. I., and R. A. Houze, Jr., 1991: Kinematic and precipitation structure of the 10-11 June 1985 squall line. *Mon. Wea. Rev.*, **119**, 3035-3065.

Biggerstaff, M. I., and R. A. Houze, Jr., 1993: Kinematics and microphysics of the transition zone of a midlatitude squall-line system. *J. Atmos. Sci.*, **50**, 3091-3110.

Churchill, D. D., and R. A. Houze, Jr., 1984: Development and structure of winter monsoon cloud clusters on 10 December 1978. *J. Atmos. Sci.*, **41**, 933-960.

Gamache, J. F., 1990: Microphysical observations in summer MONEX convective and stratiform clouds. *Mon. Wea. Rev.*, **118**, 1238-1249.

Gossard, E. E., R. G. Strauch, and R. R. Rogers, 1990: Evolution of dropsize distributions in liquid precipitation observed by ground-based Doppler radar. *J. Atmos. Ocean. Tech.*, **7**, 815-828.

Greco, S., J. Scala, J. Halverston, H. L. Massie, Jr., W. K. Tao, and M. Garstang, 1994: Amazon coastal squall lines. Part II: Heat and moisture transports. *Mon. Wea. Rev.*, **122**, 623-635.

Hallett, J., and S. C. Mossop, 1974: Production of secondary ice crystals during the riming process. *Nature*, **249**, 26-28.

Hitschfield, W., and J. Bordan, 1954: Errors inherent in the radar measurement of rainfall at attenuating wavelengths. *J. Meteor.*, **11**, 58-67.

Hobbs, P. V., S. Chang, and J. D. Locatelli, 1974: The dimensions and aggregation of ice crystals in natural clouds. *J. Geophys. Res.*, **79**, 2199-2206.

Hobbs, P. V., and A. L. Rangno, 1985: Ice particle concentrations in clouds. *J. Atmos. Sci.*, **42**, 2523-2549.

Houze, R. A., Jr., 1989: Observed structure of mesoscale convective systems and implications for large-scale heating. *Quart. J. Roy. Met. Soc.*, **115**, 425-461.

Houze, R. A., Jr., 1993: *Cloud Dynamics*. Academic Press, San Diego, 573 pp.

Houze, R. A., Jr., 1997: Stratiform precipitation in regions of convection: a meteorological paradox? *Bull. Amer. Met. Soc.*, **78**, 2179-2196.

Houze, R. A., Jr., and D. D. Churchill, 1987: Mesoscale organization and cloud microphysics in a Bay of Bengal depression. *J. Atmos. Sci.*, **44**, 1845-1867.

Hudlow, M. D., and V. L. Patterson, 1979: *GATE Radar Rainfall Atlas*, NOAA special report, 158 pp., U. S. Government Printing Office, Washington, D. C.

Keenan, T. D., L. Carey, D. Zrnic, P. May, and S. Rutledge, 1998: A sensitivity analysis of C-band polarimetric variables in rain. submitted, *J. Appl. Meteor.*

Kidder, S. Q., and T. H. Vonder Haar, 1995: *Satellite Meteorology: An Introduction*. Academic Press, San Diego, 466 pp.

Kummerow, C. 1998: Beamfilling errors in passive microwave rainfall retrievals. *J. Appl. Meteor.*, **37**, 356-370.

Lin, X., and R. H. Johnson, 1996: Heating, moistening, and rainfall over the western Pacific warm pool during TOGA COARE. *J. Atmos. Sci.*, **53**, 3367-3383.

Mapes, B. E., and R. A. Houze, Jr., 1995: Diabatic divergence profiles in western Pacific mesoscale convective systems. *J. Atmos. Sci.,* **52**, 1807-1828.

Meneghini, R., and D. Atlas, 1986: Simultaneous ocean cross section and rainfall measurements from space with nadir-looking radar. *J. Atmos. Ocean. Tech.*, **3**, 400-413.

Oguchi, T., 1983: Electromagnetic wave propagation and scattering in rain and other hydrometeors. *Proc. IEEE*, **71**, 1029-1078.

Pruppacher, H. R., and J. D. Klett, 1978: *Microphysics of Clouds and Precipitation*. D. Reidel Publishers, Dordrecht, 714 pp.

Reed, R. J., and E. E. Recker, 1971: Structure and properties of synoptic-scale wave disturbances in the equatorial western Pacific. *J. Atmos. Sci.*, **28**, 1117-1133.

Ryzhkov, A., and D. S. Zrnic, 1995: Precipitation and attenuation measurements at a 10-cm wavelength. *J. Appl. Meteor.*, **34**, 2121-2134.

Sachidananda, M., and D. S. Zrnic, 1987: Rain rate estimates from differential polarization measurements. *J. Atmos. Ocean Tech.*, **4**, 588-598.

Short, D. A., P. A. Kucera, B. S. Ferrier, J. C. Gerlach, S. A. Rutledge, and O. W. Thiele, 1997: Shipboard radar rainfall patterns within the TOGA COARE IFA. *Bull. Amer. Meteor. Soc.*, **78**, 2817-2836.

Smith, E. A., A. Mugnai, H. J. Cooper, G. J. Tripoli, and X. Xiang, 1992: Foundations for statistical-physical precipitation retrieval from passive microwave satellite measurements. Part I: Brightness-temperature properties of a time-dependent cloud radiation model. *J. Applied. Meteor*, **31**, 506-531.

Smith, E. A, J. E. Lamm, R. Adler, J. Alishouse, K. Aonashi, E. Barrett, P. Bauer, W. Berg, A. Chang, R. Ferraro, J. Ferriday, S. Goodman, N. Grody, C. Kidd, D. Kniveton, C. Kummerow, G. Liu, F. Marano, A. Mugnai, W. Olson, G. Petty, A. Shibata, R. Spencer, F. Wentz, T. Wilheit and E. Zipser, 1999: Results of the WetNet PIP-2 project. *J. Atmos. Sci.*, in press.

Steiner, M., R. A. Houze, Jr., and S. E. Yuter, 1995: Climatological characterization of three-dimensional storm structure from operational radar and rain gauge data. *J. Appl. Meteor.*, **34**, 1978-2007.

Tao, W.-K., and J. Simpson, 1993: The Goddard Cumulus Ensemble Model. Part I: Model description. *Terrestrial, Atmospheric and Oceanic Sciences*, **4**, 35-72.

Tokay, A., and D. A. Short, 1996: Evidence from tropical raindrop spectra of the origin of rain from stratiform versus convective clouds. *J. Appl. Meteor.*, **35**, 355-371.

Wakasugi, K., A. Mizutani, M. Matsuo, S. Fukao, and S. Kato, 1986: A direct method of deriving drop-size distribution and vertical air velocities from VHF Doppler radar spectra. *J. Atmos. Ocean. Tech.*, **3**, 623-629.

Waldvogel, A., 1974: The N_O jump in raindrop spectra. *J. Atmos. Sci.*, **31**, 1067-1078.

Wallace, J. M., and P. V. Hobbs, 1977: *Atmospheric Science: An Introductory Survey*. Academic Press, New York, 467 pp.

Wilheit, T. T., 1986: Some comments on passive microwave measurement of rain. *Bull. Amer. Meteor. Soc.*, **67**, 1226-1232.

Yanai, M. S., S. Esbensen, and J.-H. Chu, 1973: Determination of bulk properties of tropical clouds clusters from large-scale heat and moisture budgets. *J. Atmos. Sci.*, **30**, 611-627.

Yuter, S. E., and R. A. Houze, Jr., 1995: Three-dimensional kinematic and microphysical evolution of Florida cumulonimbus, Part II: Frequency distributions of vertical velocity, reflectivity, and differential reflectivity. *Mon. Wea. Rev.*, **123**, 1941-1963.

Yuter, S. E., and R. A. Houze, Jr., 1997: Measurements of raindrop size distributions over the Pacific warm pool and implications for *Z*-*R* relations. *J. Appl. Meteor.*, **36**, 847-867.

Zipser, E. J., 1994: Deep cumulonimbus cloud systems in the tropics with and without lightning. *Mon. Wea. Rev.*, **122**, 1837-1851.

Table 1. Mapping of specific types of measurements to scientific objectives by section. Relative scale of importance of measurement to objective on scale from 1 to 10. v refers to validation portion of objective and i refers to initialization portion of objective.

Scientific Objectives

Type of Measurement

	RTC input (1.2.3)	RTC inhom (1.2.4)	PR (1.3)	conv/ sf (1.4.1)	precip struct (1.4.2)	sfc precip (1.4.4)	budget (1.6)	cloud model (1.5)
Horiz Divergence Profiles								
at 500m-2 km res in 3D vol	6	6	6	10	8	8	10	10v
over areas							10	10v
Vertical Velocity								
at 500m-2km res in 3d vol	5	10	10	7	8	8	10	10v
along flight tracks					8	8	5v	8v
Thermodynamic Profiles								
sfc to stratosphere	10	3	0	0	5	2	9	10i
boundary layer	10	3	0	0	5	2	10	10i
within precip regions	10	3	0	0	8	2	5	8v
budget over closed array	8	NA	0	6	2	9	10	10vi
Horiz spatial variability of water vapor at low levels	5	3	0	4	1	0	10	9vi
Surface evaporation	0	0	0	0	0	0	10	9i
Surface temperature (SST)	7	0	1	0	5	0	10	8i
Surface wind	7	3	10	0	5	7	10	8v
Incoming microwave radiation	4	4	0	0	0	0	0	0
Depth of rain layer	10	7	10	8	10	8	0	5v
Microwave scattering of regions with high concs of ice and large ice at TMI freq								
Upward	10	10	0	0	0	0	0	0
Downward	0	0	0	0	0	0	0	0
Microwave absorption of rain regions at TMI freq								
Upward	10	10	5	0	0	0	0	0
Downward	10	10	5	0	0	0	0	0
Mixing ratios and num. conc. with height and their spatial variability within precipitating cloud:								
water vapor	10	4	0	5	0	0	5	10vi
cloud water	8	4	0	8	0	0	0	10v
cloud ice	4	4	0	0	0	0	0	10v
rain	10	10	10	10	10	10	0	9v
snow (aggregates)	10	10	7	10	10	8	0	10v
graupel	10	10	7	10	10	8	0	10v
Drop size distributions								
fine res vertical profiles	10	10	10	10	10	10	0	8vi
fine res horiz variability	10	10	10	10	10	10	0	5v
Graupel detection	NA	NA	NA	8	9	0	0	8v
3D vols of non-attenuated Z	8	10	10	10	10	6	0	10v
Surface rain rates	10	10	10	7	10	10	10	10v
3D volumes of ZDR, KDP and ρ_{hv}	0	6	6	8	10	10	0	10v

Table 2. Basic characteristics of nominal Kwajalein TRMM GV radar scan strategy.

a)

name	variables	Scan speed (deg/sec)	# tilts	# samples	bin spacing (m)	Max range (km)	PRF (Hz)	Nyquist velocity (m/s)
survellience	Z	8	1	50	250	378.5	396	NA
Non-pol volume	Z, Vr	18	22	52	250	160.5	934	25.0
dual-pol A volume	Z, Vr, ZDR, PHIDP	8	11	116 (58 H/ 58 V)	250	160.5	934	25.0
dual-pol B volume	Z, Vr, ZDR, PHIDP	8	11	116 (58 H/ 58 V)	250	160.5	934	25.0

b)

scan name	set of elevation angles (deg)
surveillance	1
non-pol volume	0.4, 0.65, 0.9, 1.2, 1.5, 1.9, 2.3, 2.7, 3.1, 3.5, 4.3, 5.2, 6.0, 7.0, 8.1, 9.5, 11.1, 13.2, 15.7, 18.9, 23.1, 28.8
dual-pol A volume	0.4, 1.2, 1.9, 2.7, 3.5, 5.2, 7.0, 9.5, 13.2, 18.9, 28.8
dual-pol B volume	0.4, 0.9, 1.5, 2.3, 3.1, 4.3, 6.0, 8.1, 11.1, 15.7, 23.1

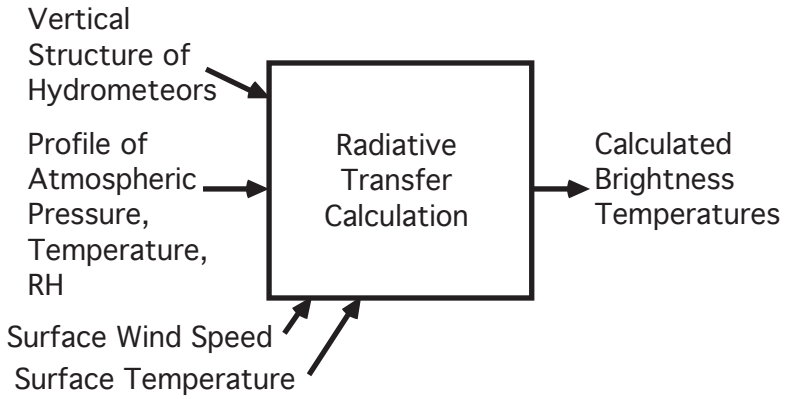

Figure 1. Illustration of the radiative transfer calculation input and outputs.

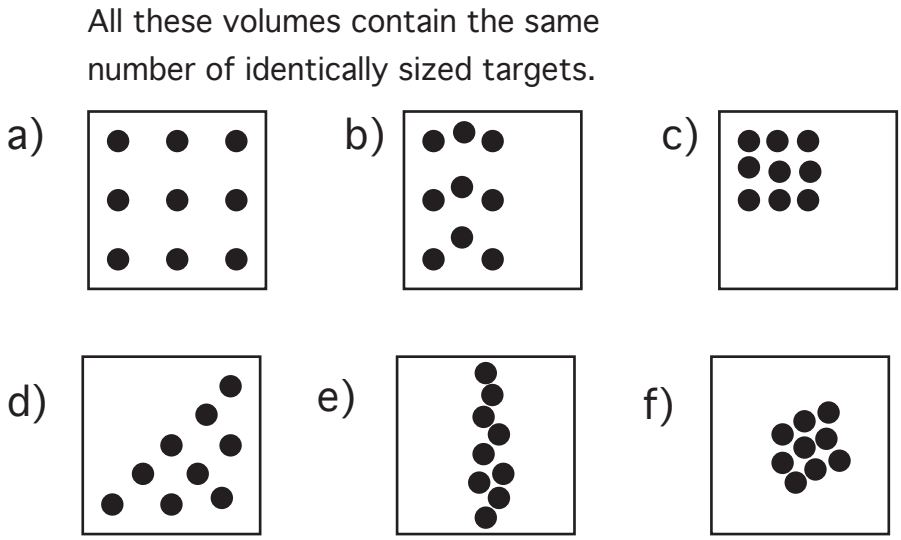

Figure 2. Conceptual illustration of the beam filling issue.

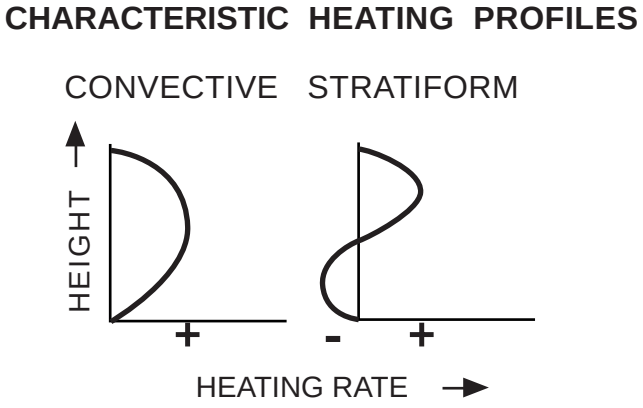

Figure 3. Characteristic heating profiles for convective and stratiform regions.

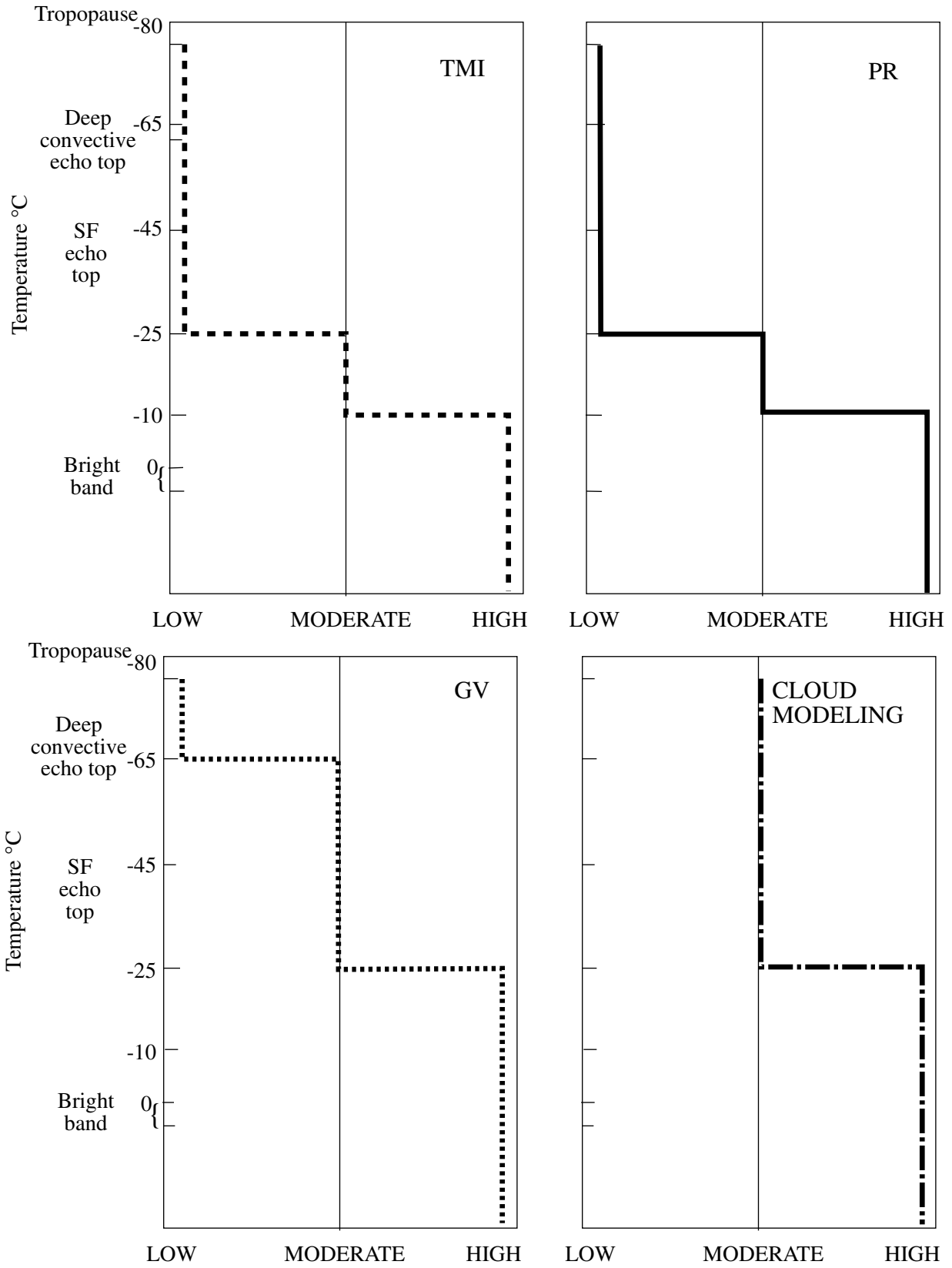

Figure 4. The relative interest in microphysical measurements at various altitudes by the TMI, PR, GV, and cloud modeling facets of KWAJEX.

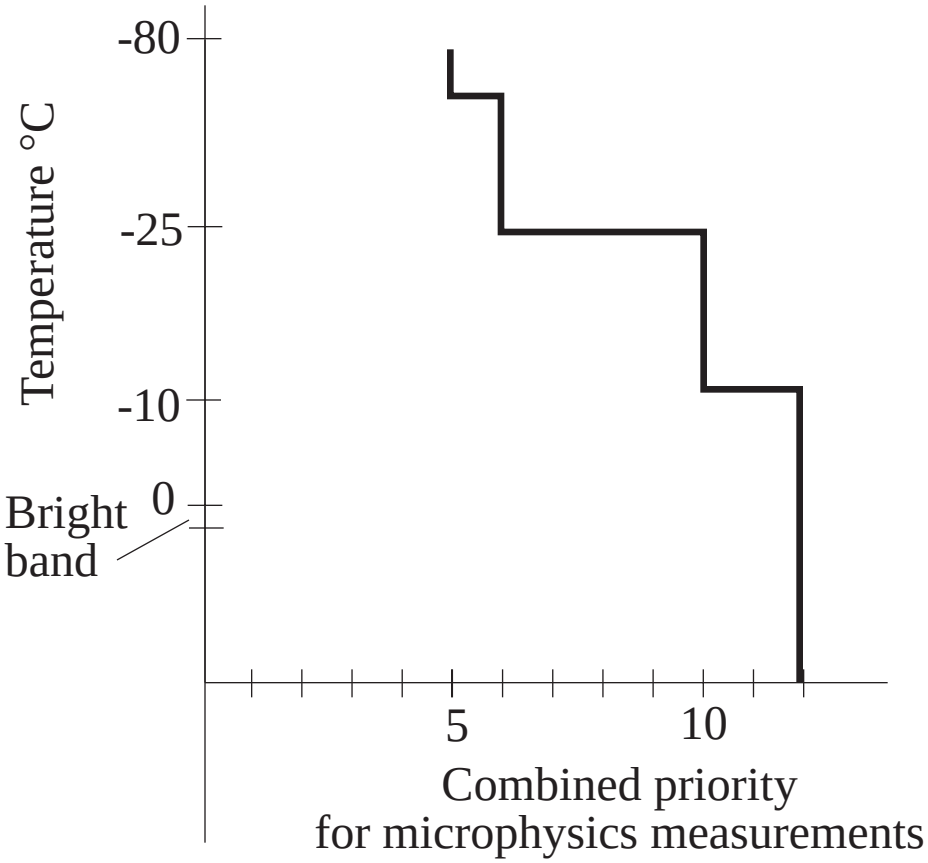

Figure 5. The net relative interest in microphysical measurement at various altitudes derived from Fig. 4.

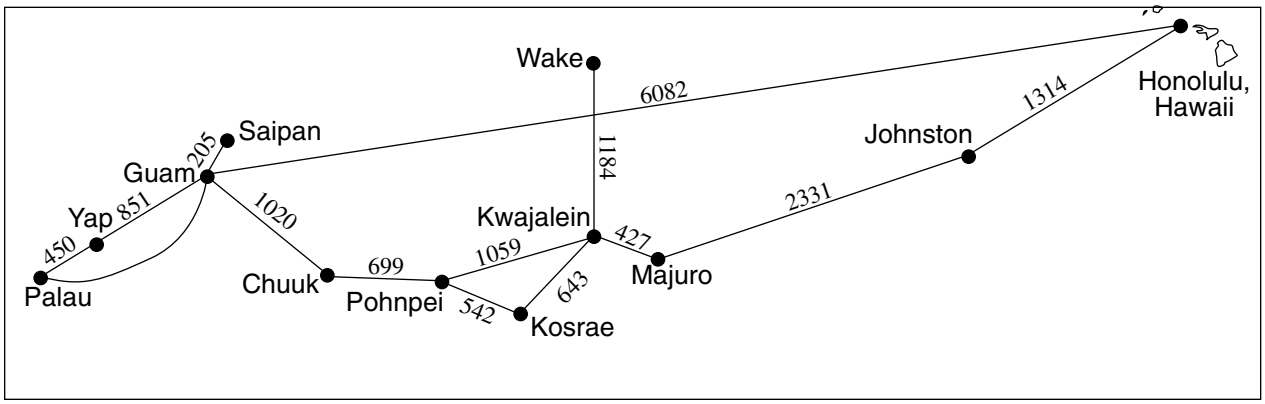

Figure 6. Map of central Pacific showing distances in km between various islands. Distance is in km.

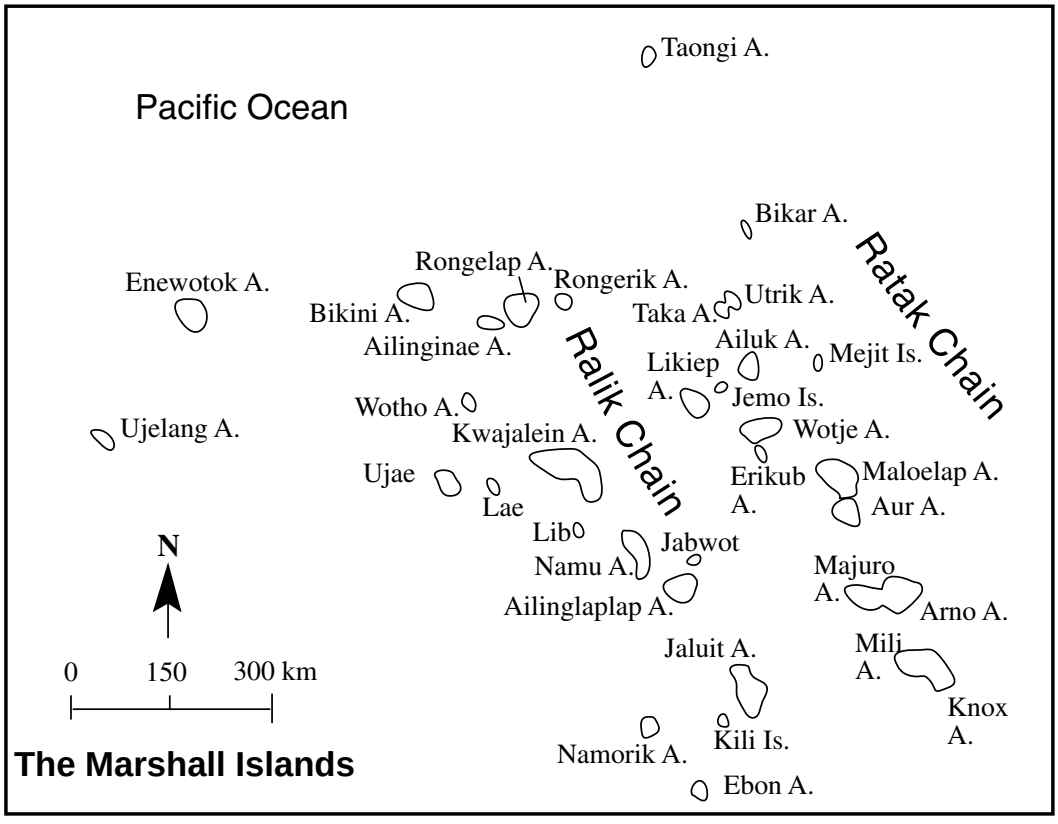

Figure 7. Map of atolls within the Marshall Islands.

Kwajalein Atoll, Marshall Islands

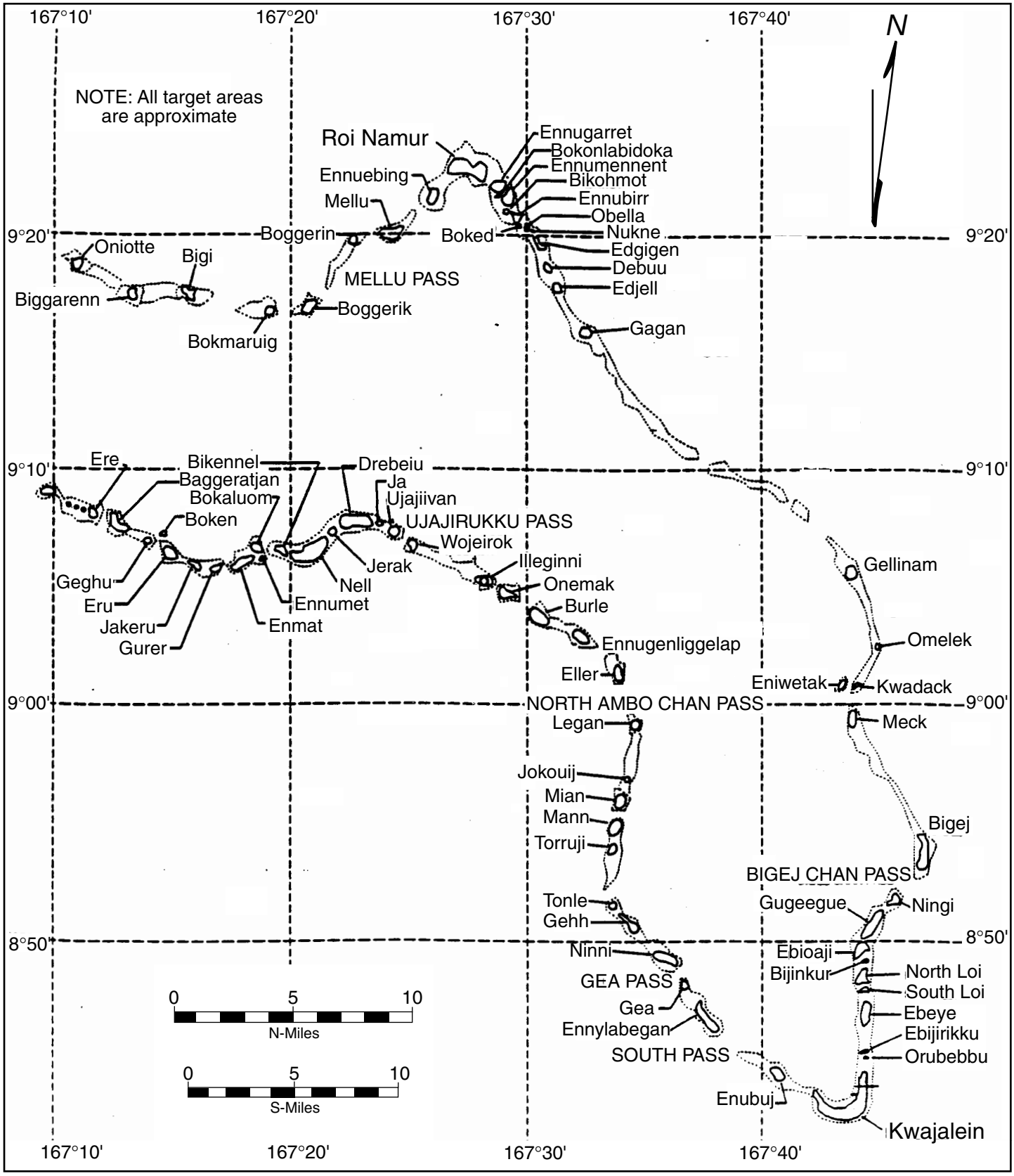

Figure 8. Map of islands in the eastern portion of Kwajalein Atoll.

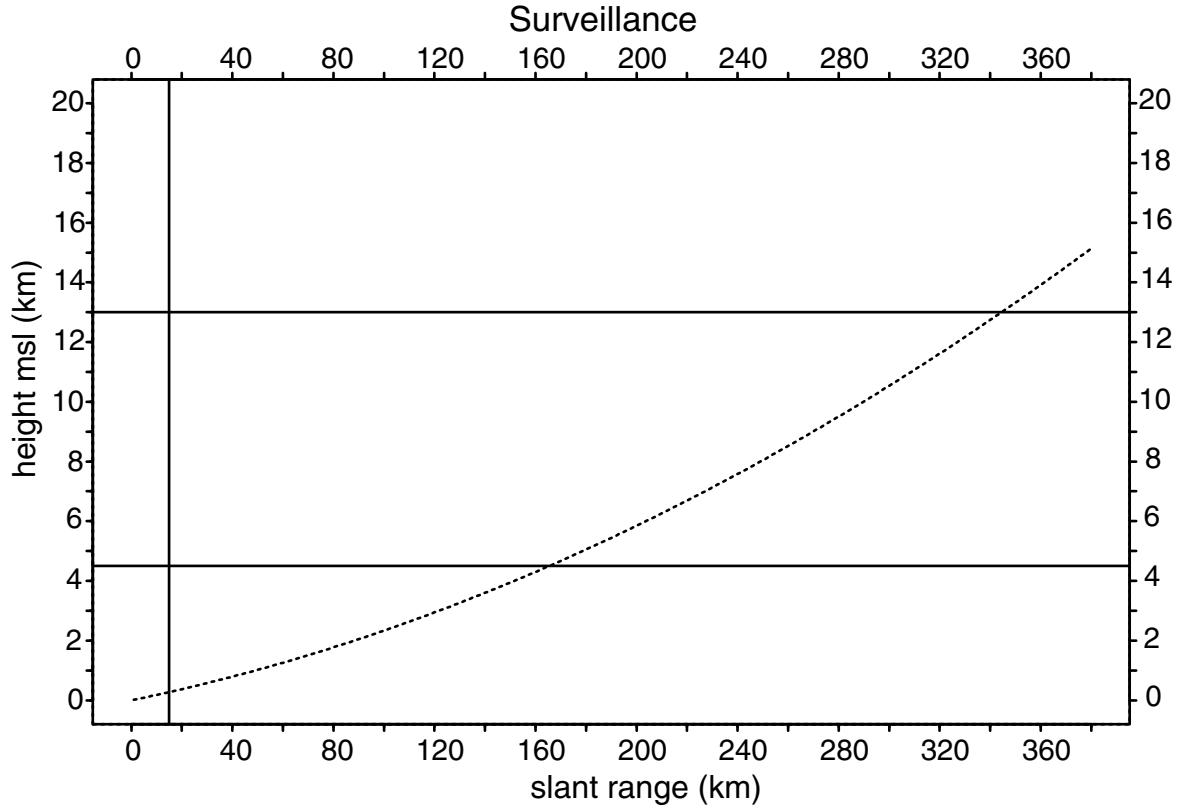

Figure 9. Range-height plot of 1° elevation angle surveillance scan to 380 km range. Minimum range for useable echo is 15 km. Height of freezing level (4.5 km) and nominal maximum echo top height (13 km) are indicated.

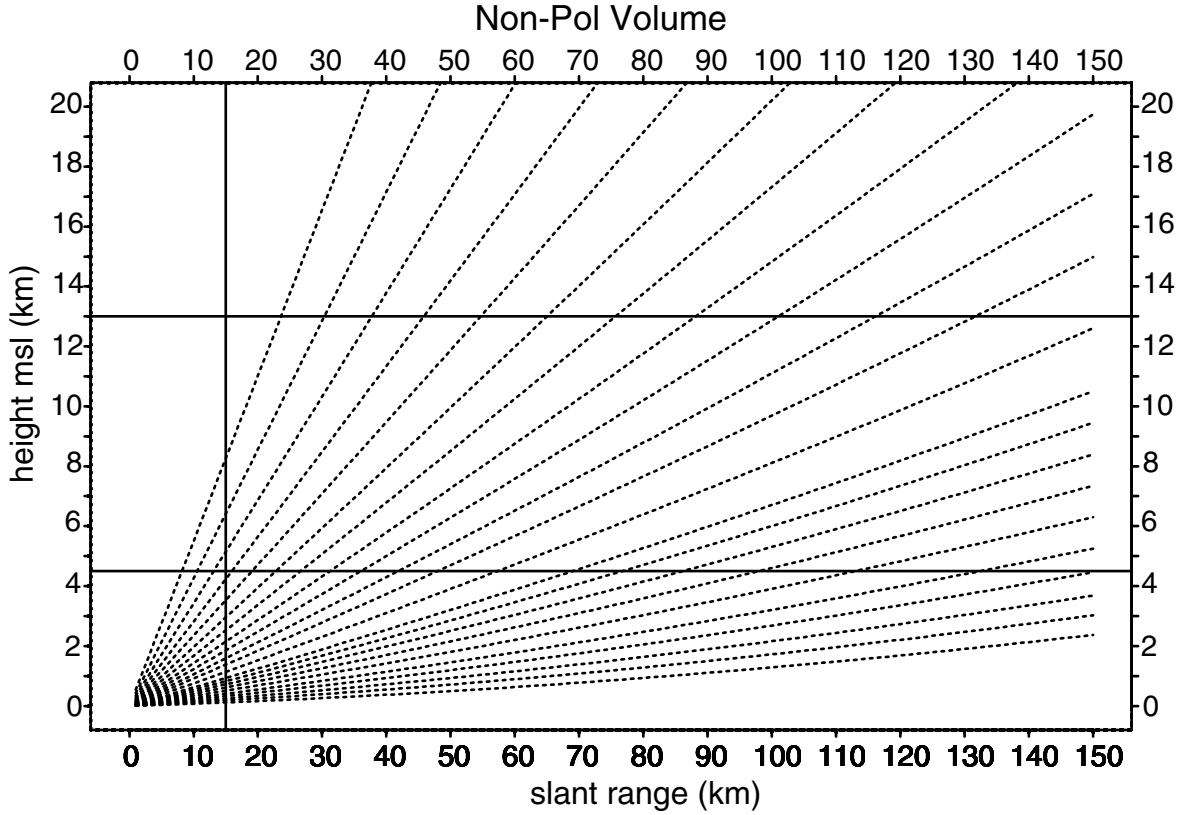

Figure 10. Range-height plot of elevation angles in nonpolarization volume scan (Table 2) to 150 km range. Minimum range for useable echo is 15 km. Height of freezing level (4.5 km) and nominal maximum echo top height (13 km) are indicated.

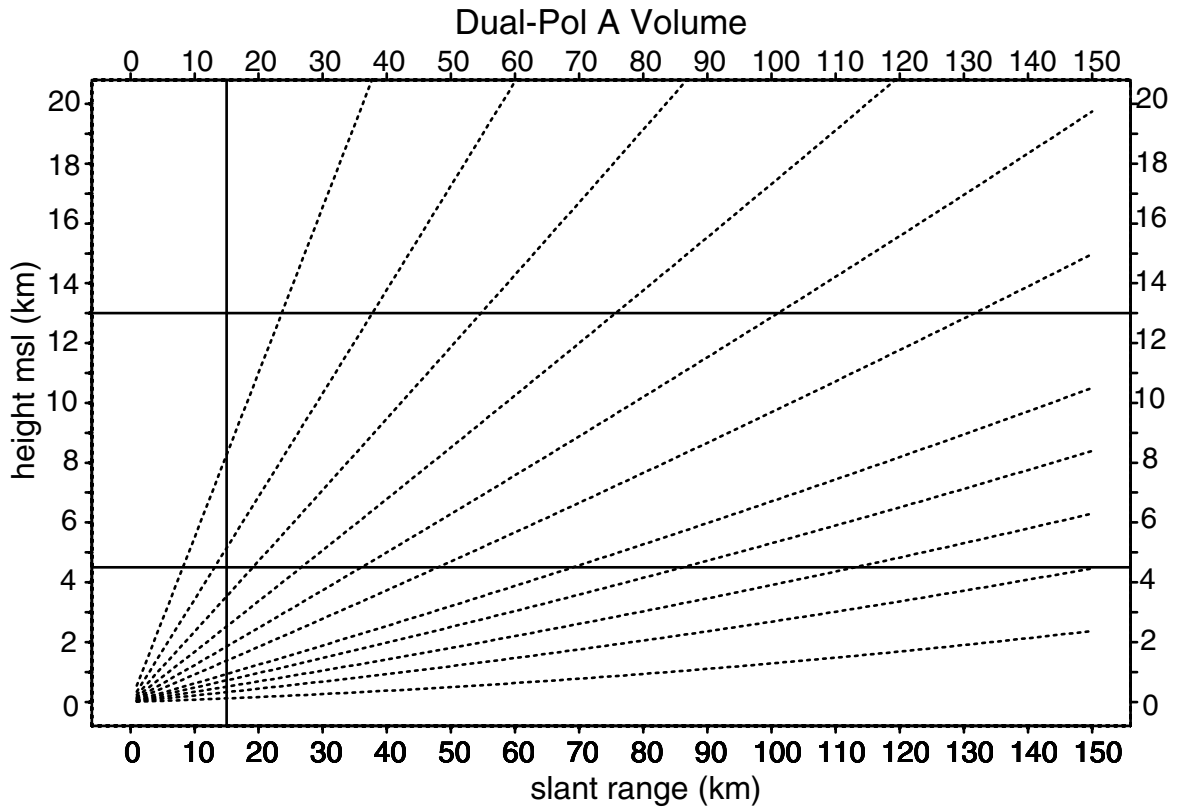

Figure 11. As in Fig. 10 except for elevation angles in dual-polarization volume scan A (Table 2).

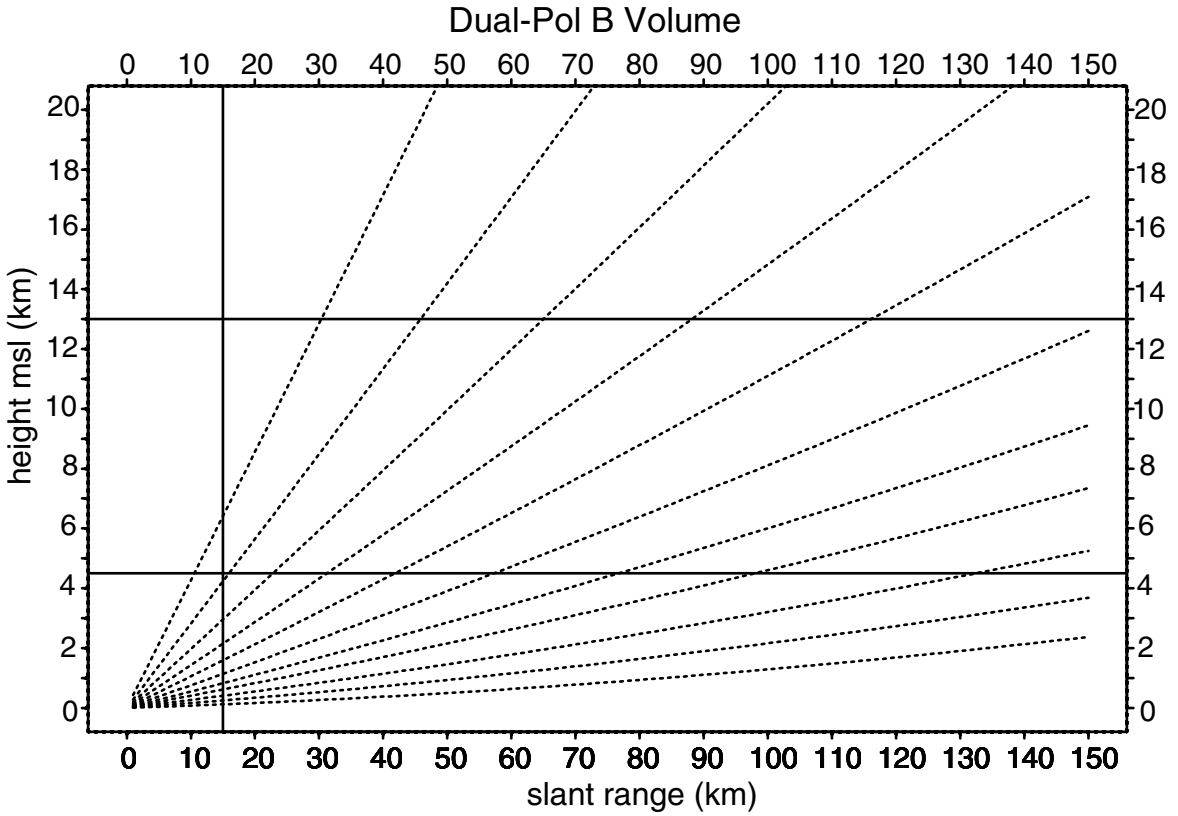

Figure 12. As in Fig. 10 except for elevation angles in dual-polarization volume scan B (Table 2).

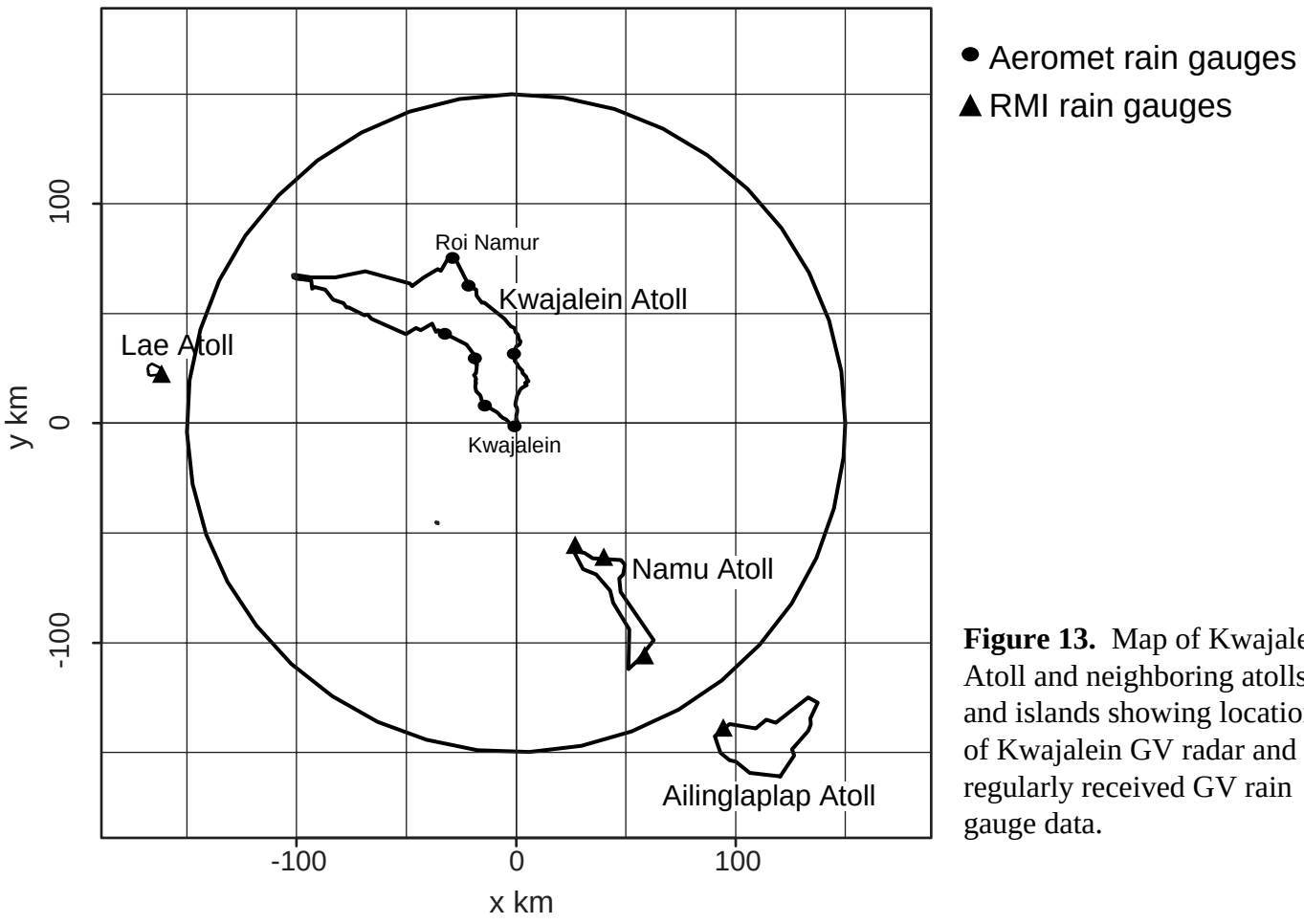

Figure 13. Map of Kwajalein Atoll and neighboring atolls and islands showing location of Kwajalein GV radar and regularly received GV rain gauge data.

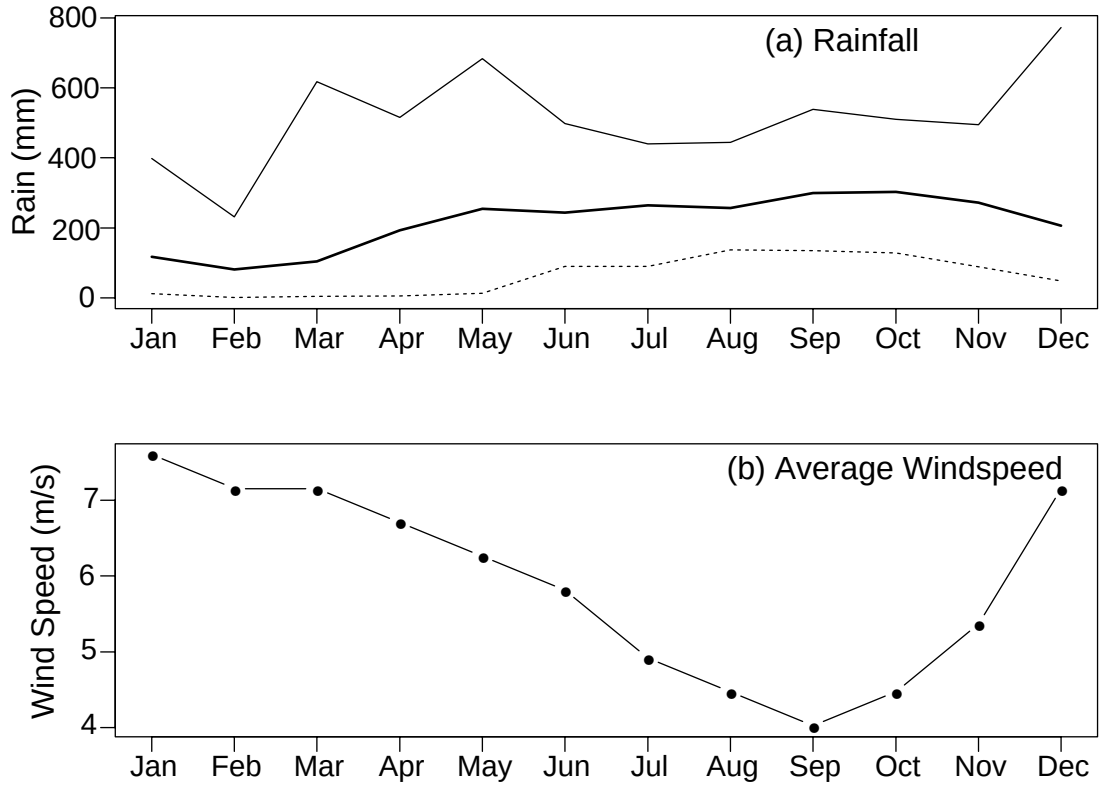

Figure 14. Kwajalein climatological data based on records from 1945-1993. a) Monthly precipitation, average (thick line), maximum (thin line), minimum dotted line. b) Average wind speed. (Data courtesy of Aeromet Inc.)

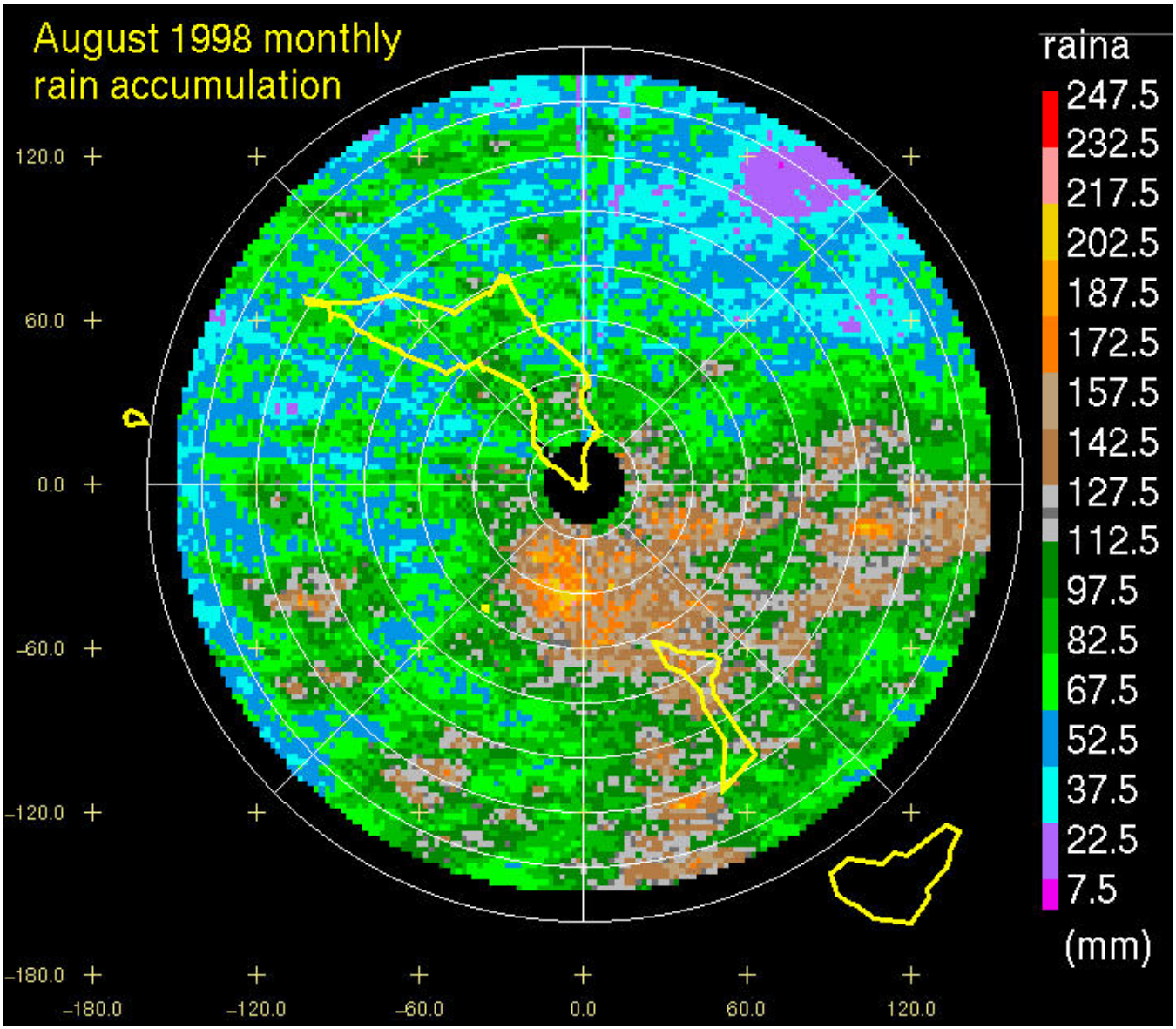

Figure 15. Monthly precipitation accumulation in mm for Kwajalein GV region during period of radar operations during August 1998 similar to TRMM GV product 3A-54.

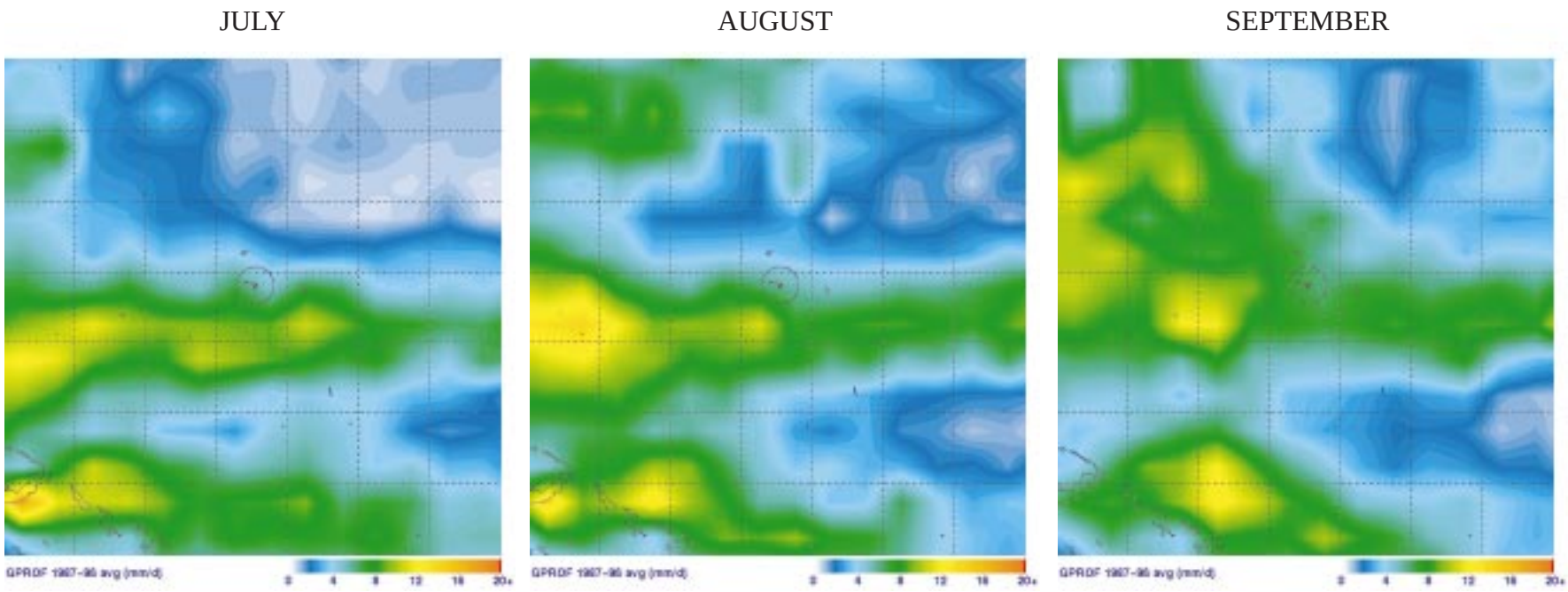

Figure 16. Average monthly precipitation in western Pacific derived from satellite SSM/I data using GPROF (Goddard Profiling Algorithm) for period 1987-1996. The 150 km radius TRMM GV area centered on Kwajalein Island is indicated by the circle in the center of the figure. (Figure courtesy of C. Kummerow and E. Nelkin.)

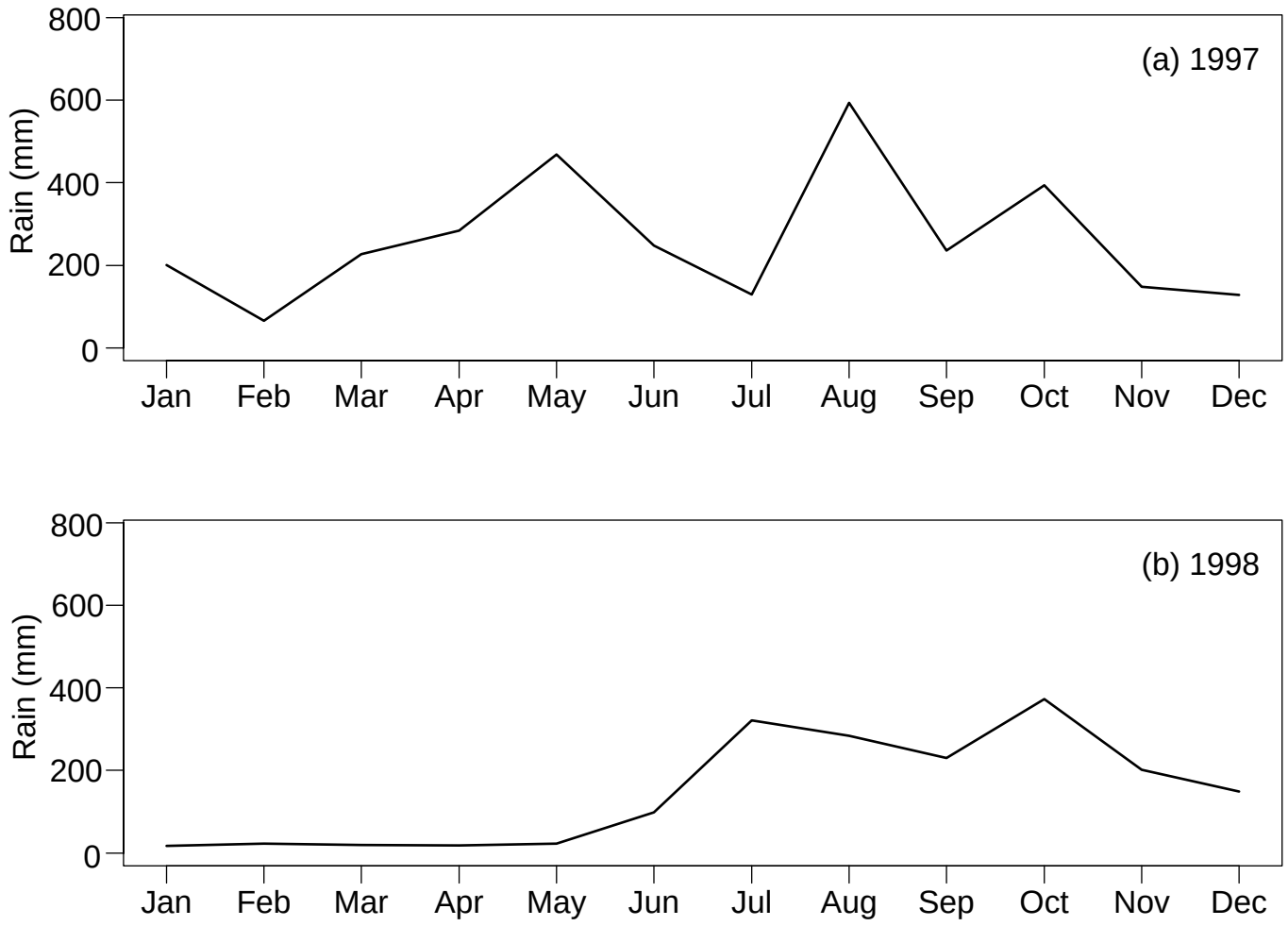

Figure 17. Recorded monthly rainfall at Kwajalein Island for 1997 and 1998. (Data courtesy of Aeromet Inc.)

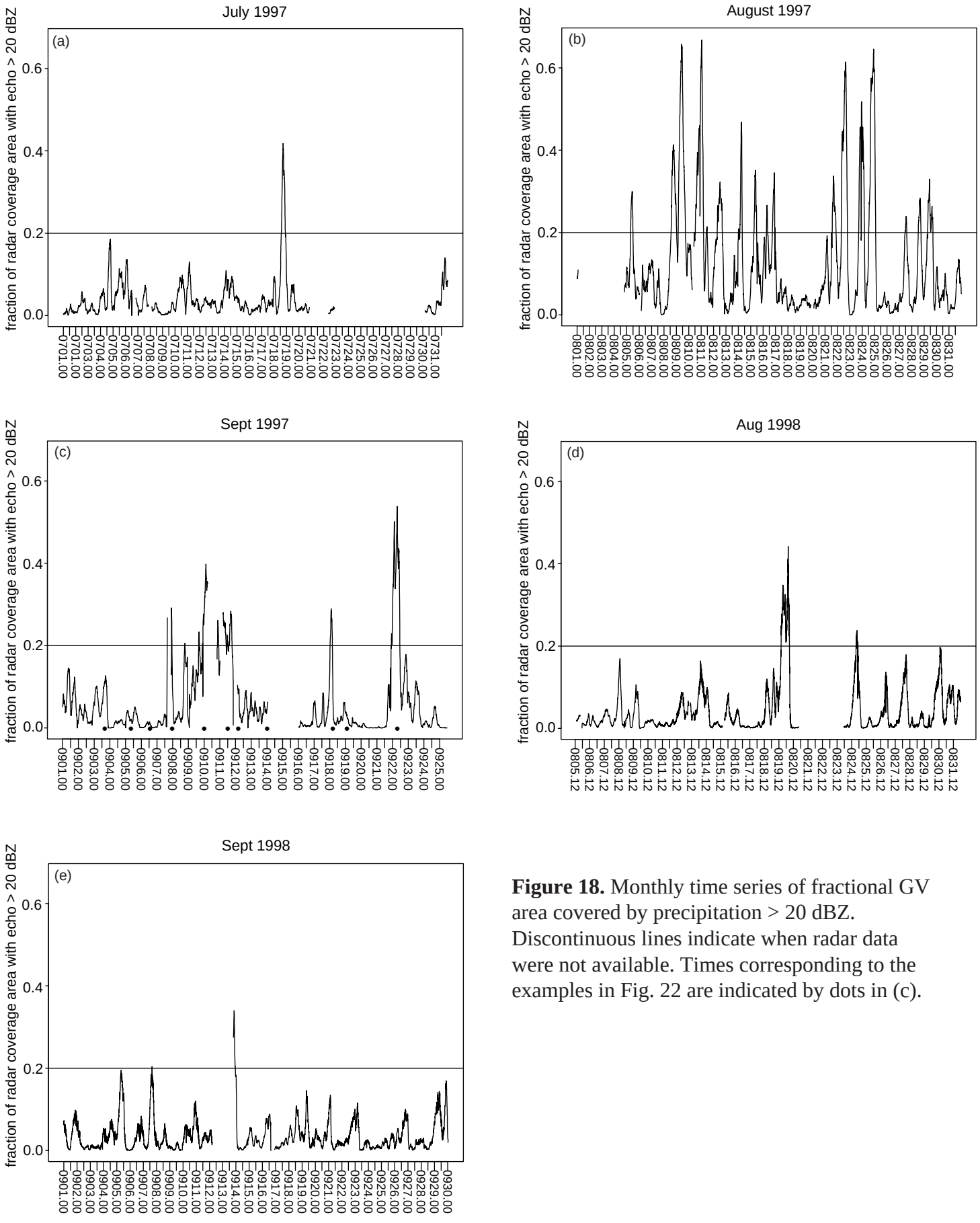

Figure 18. Monthly time series of fractional GV area covered by precipitation > 20 dBZ. Discontinuous lines indicate when radar data were not available. Times corresponding to the examples in Fig. 22 are indicated by dots in (c).

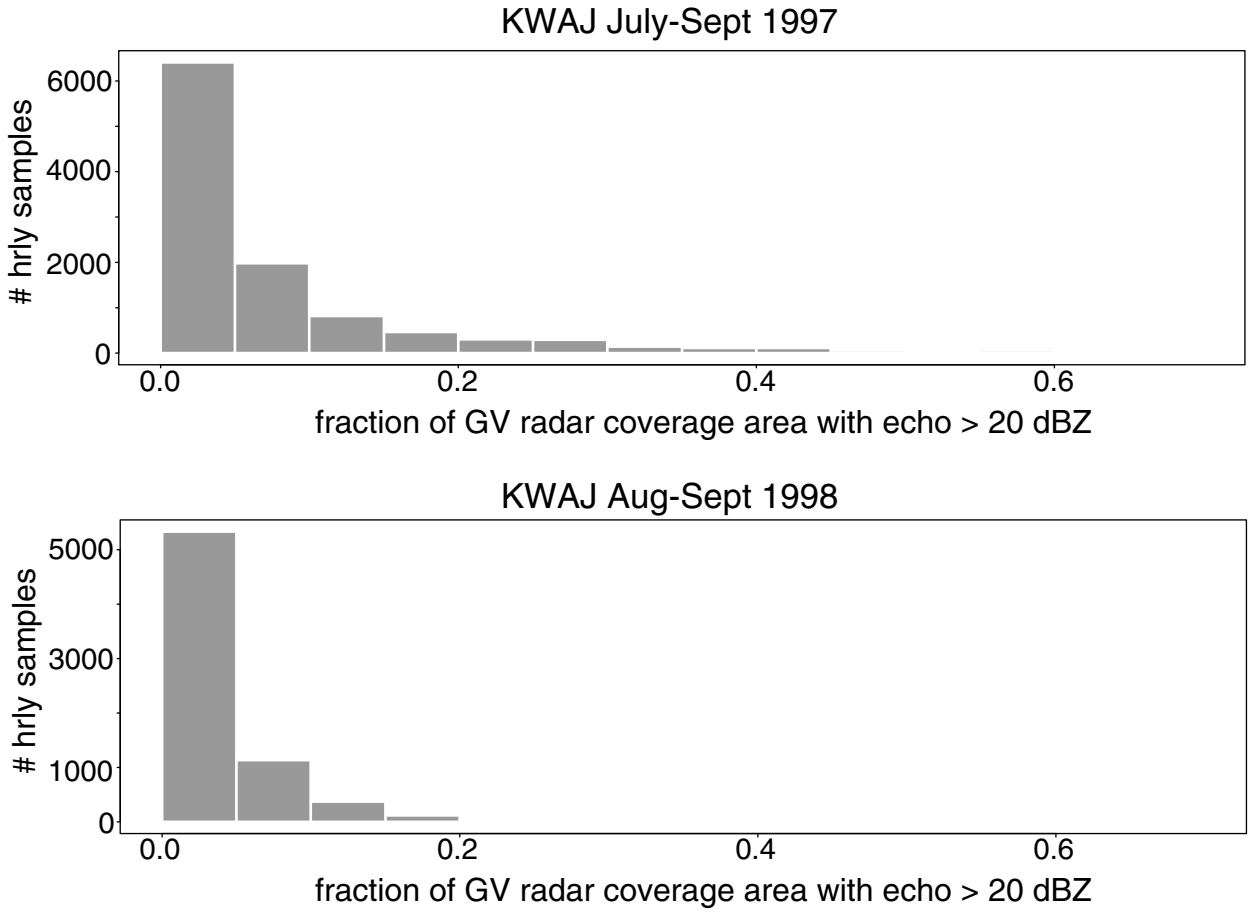

Figure 19. Histogram of the fraction of areal coverage of precipitation > 20 dBZ within the GV region tabulated at intervals of 5%.

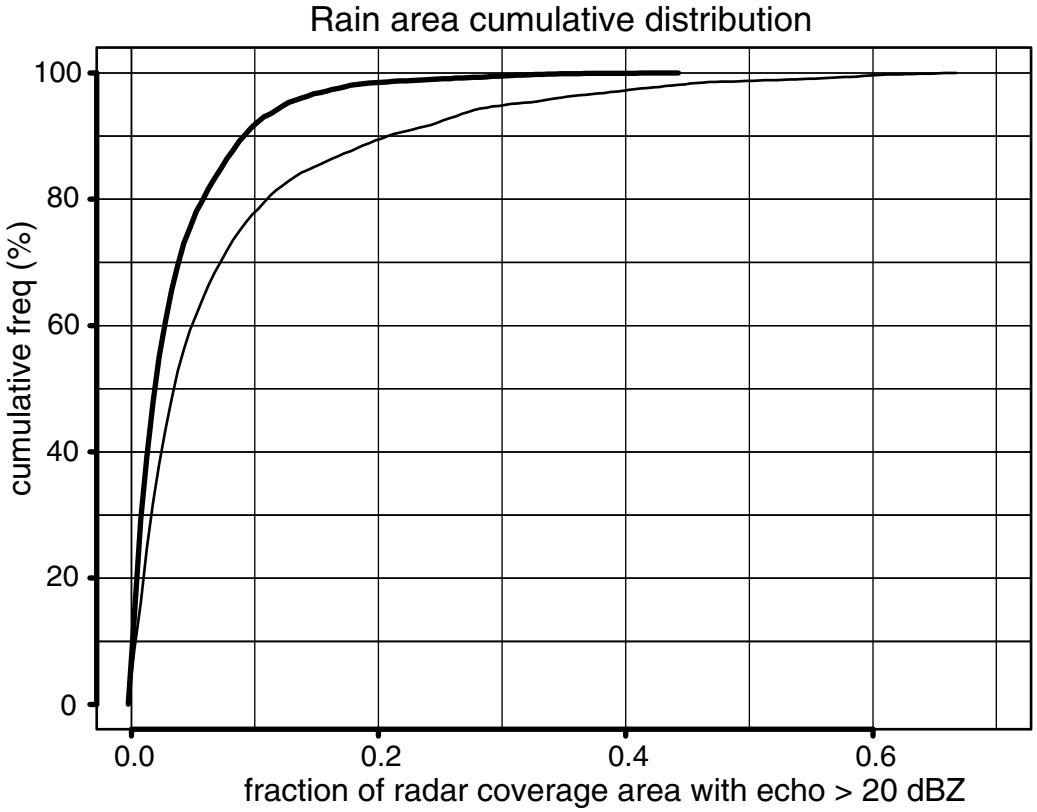

Figure 20. Cumulative frequency as a function of instantaneous precipitating area. July, August, and September 1997 - thin line, August and September 1998 - heavy line.

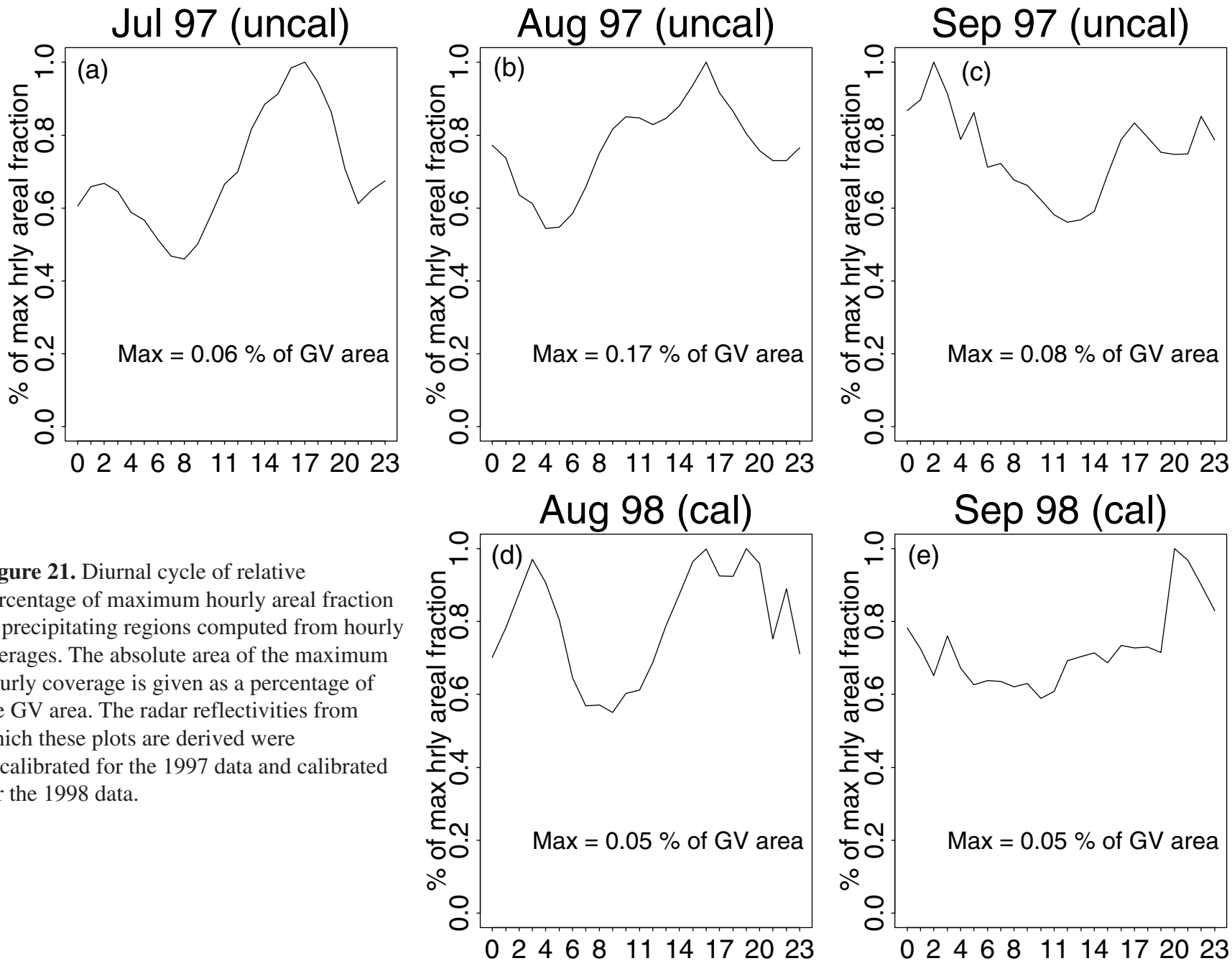

Figure 21. Diurnal cycle of relative percentage of maximum hourly areal fraction of precipitating regions computed from hourly averages. The absolute area of the maximum hourly coverage is given as a percentage of the GV area. The radar reflectivities from which these plots are derived were uncalibrated for the 1997 data and calibrated for the 1998 data.

(a)

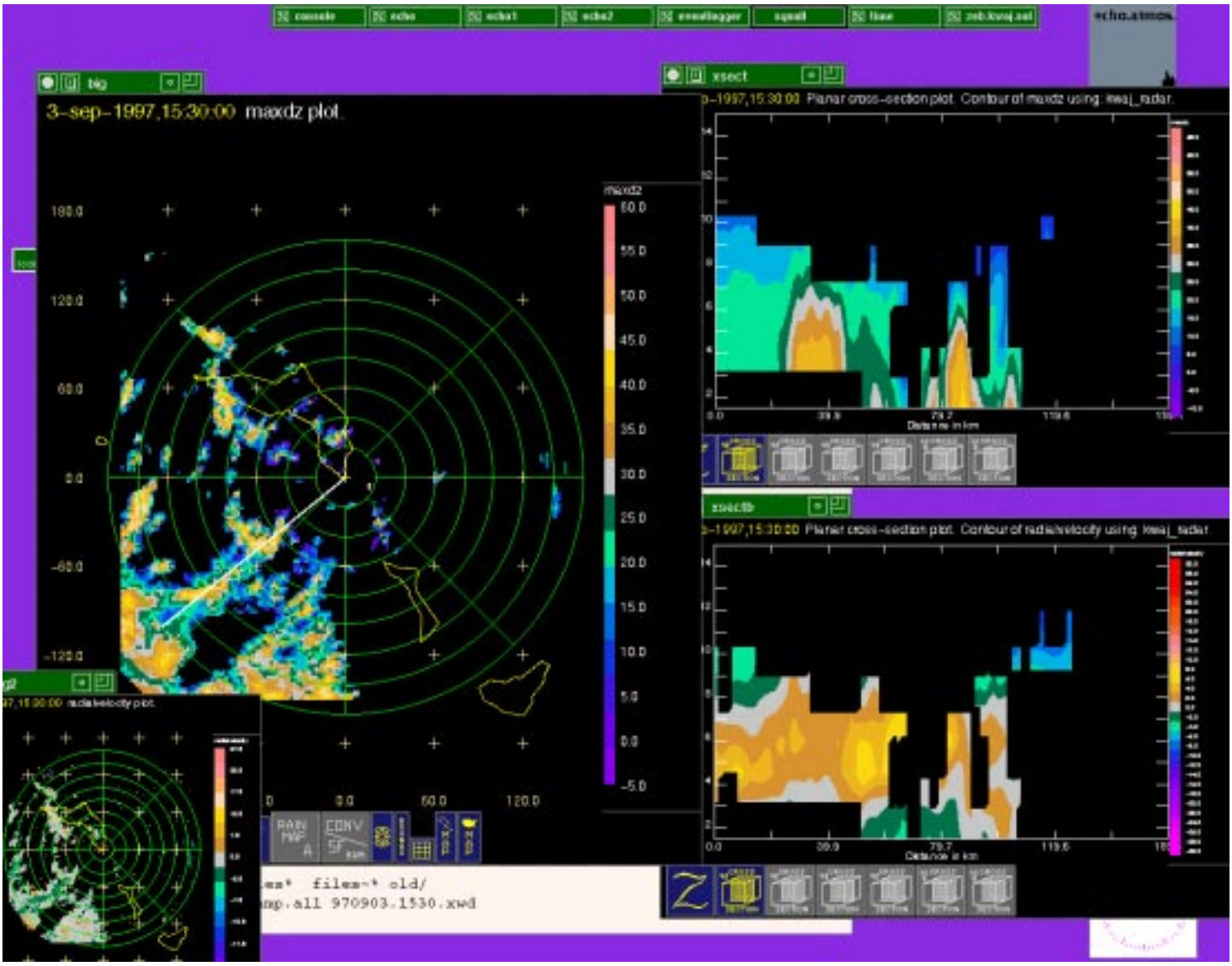

Figure 22. (a-k) Examples of precipitation patterns at Kwajalein from September 1997.

(b)

Figure 22. (continued)

(c)

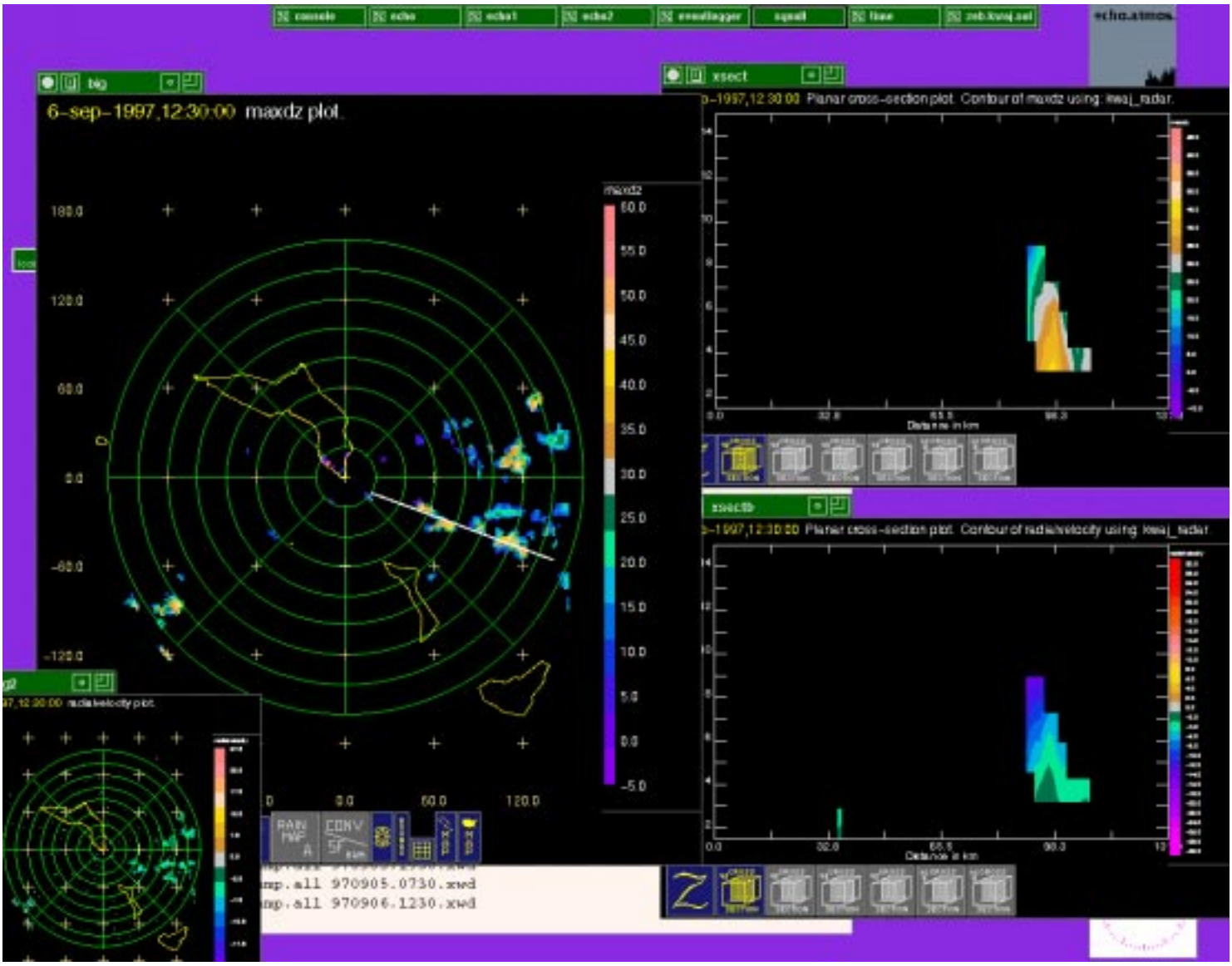

Figure 22. (continued)

(d)

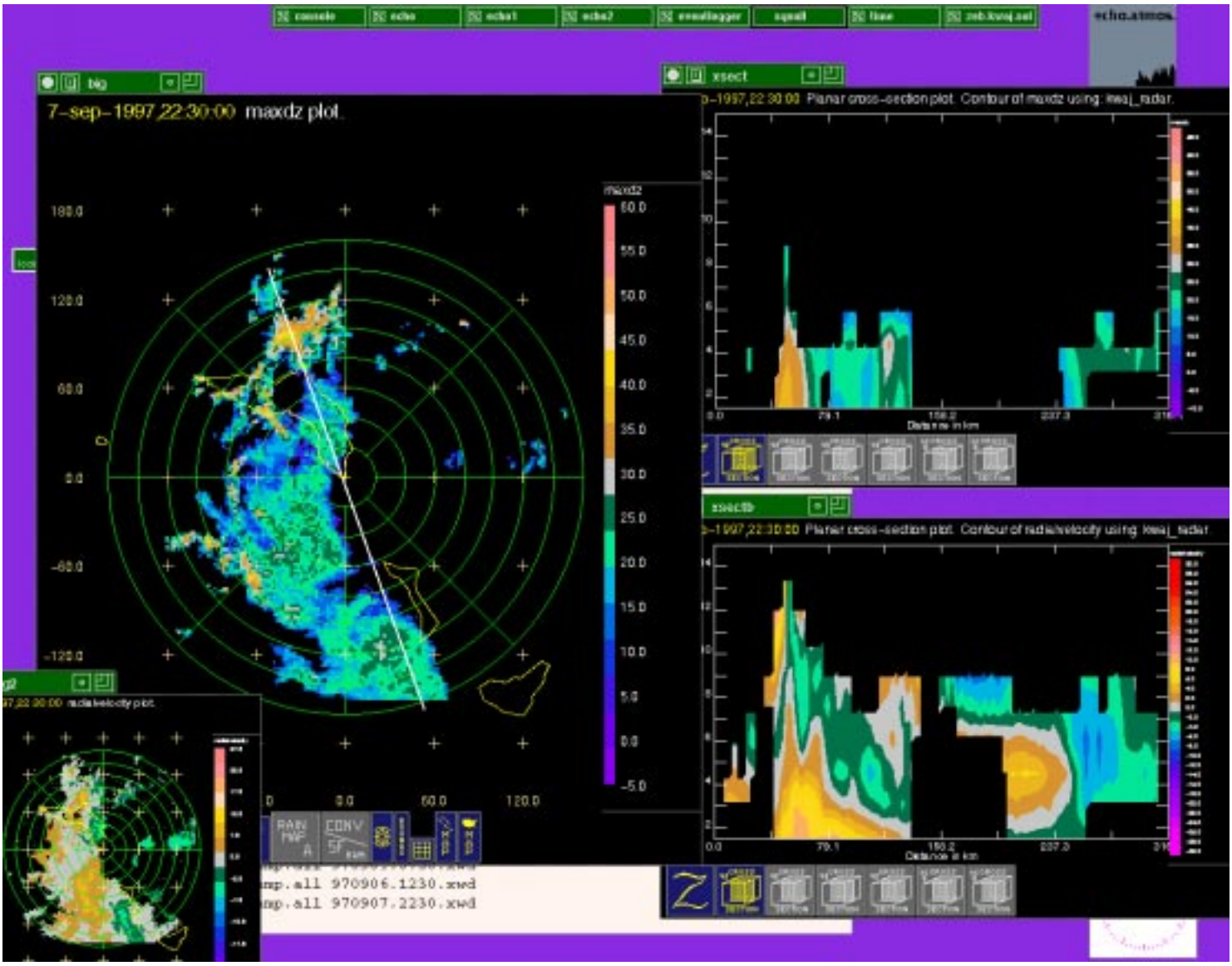

Figure 22. (continued)

(e)

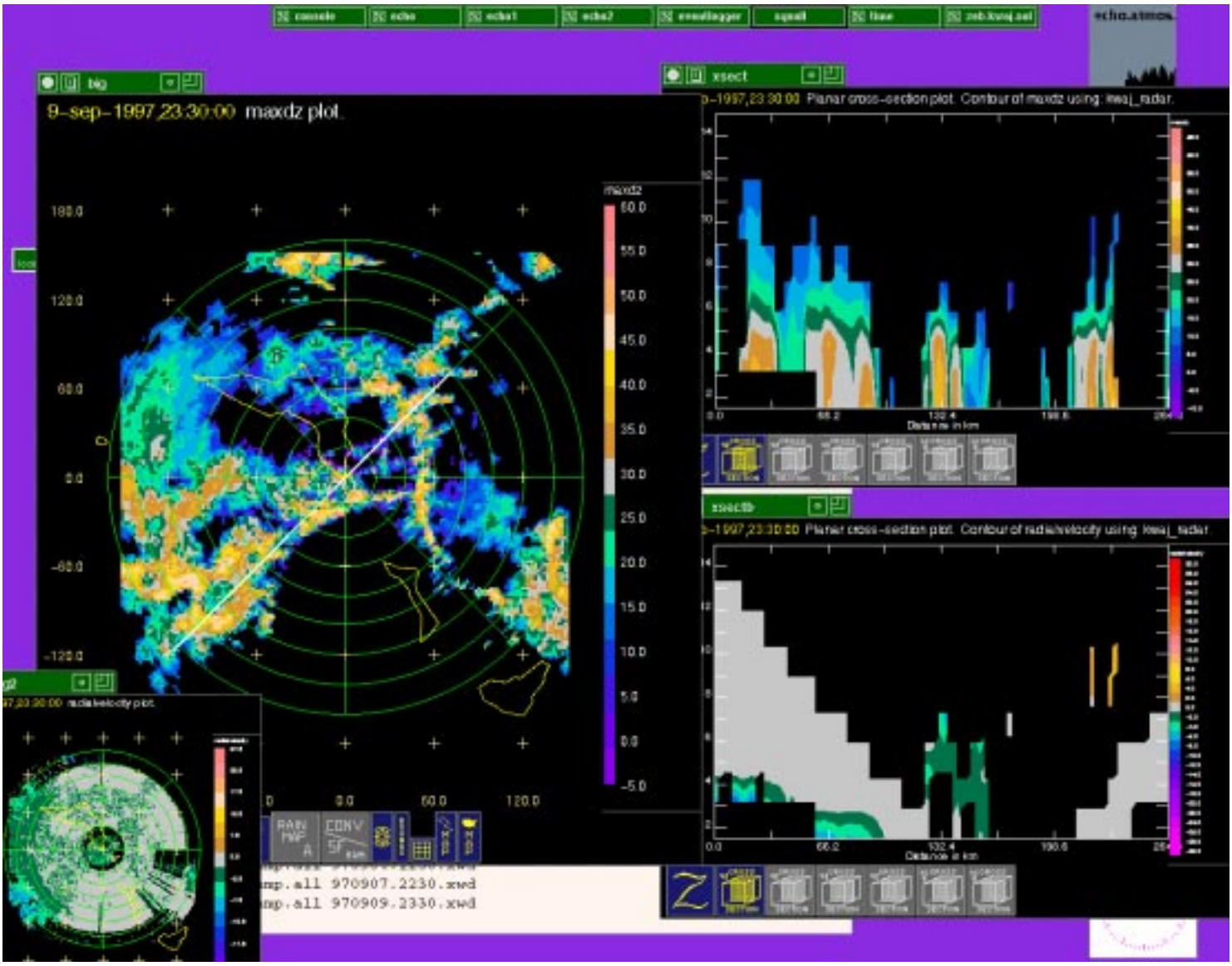

Figure 22. (continued)

(f)

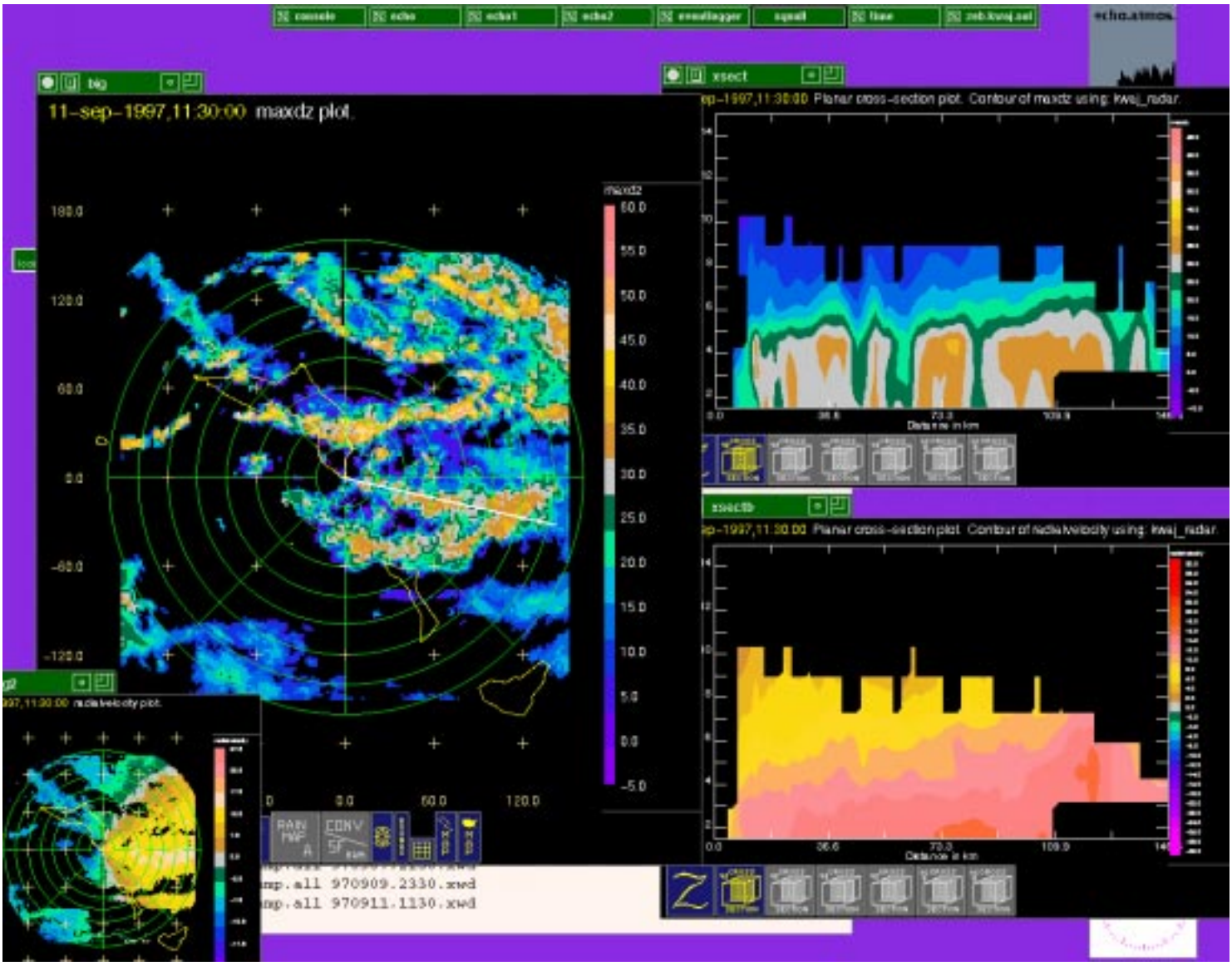

Figure 22. (continued)

(g)

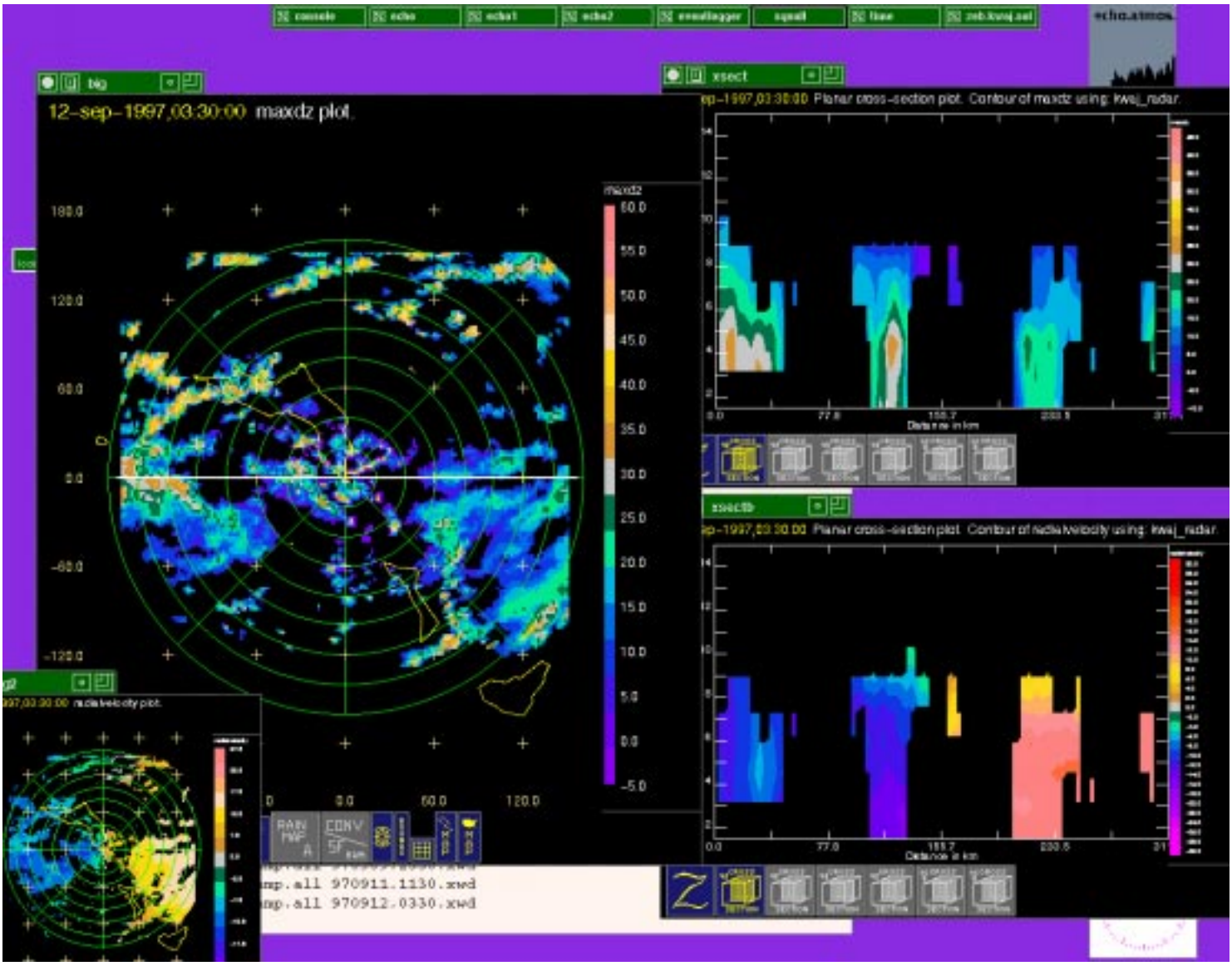

Figure 22. (continued)

(h)

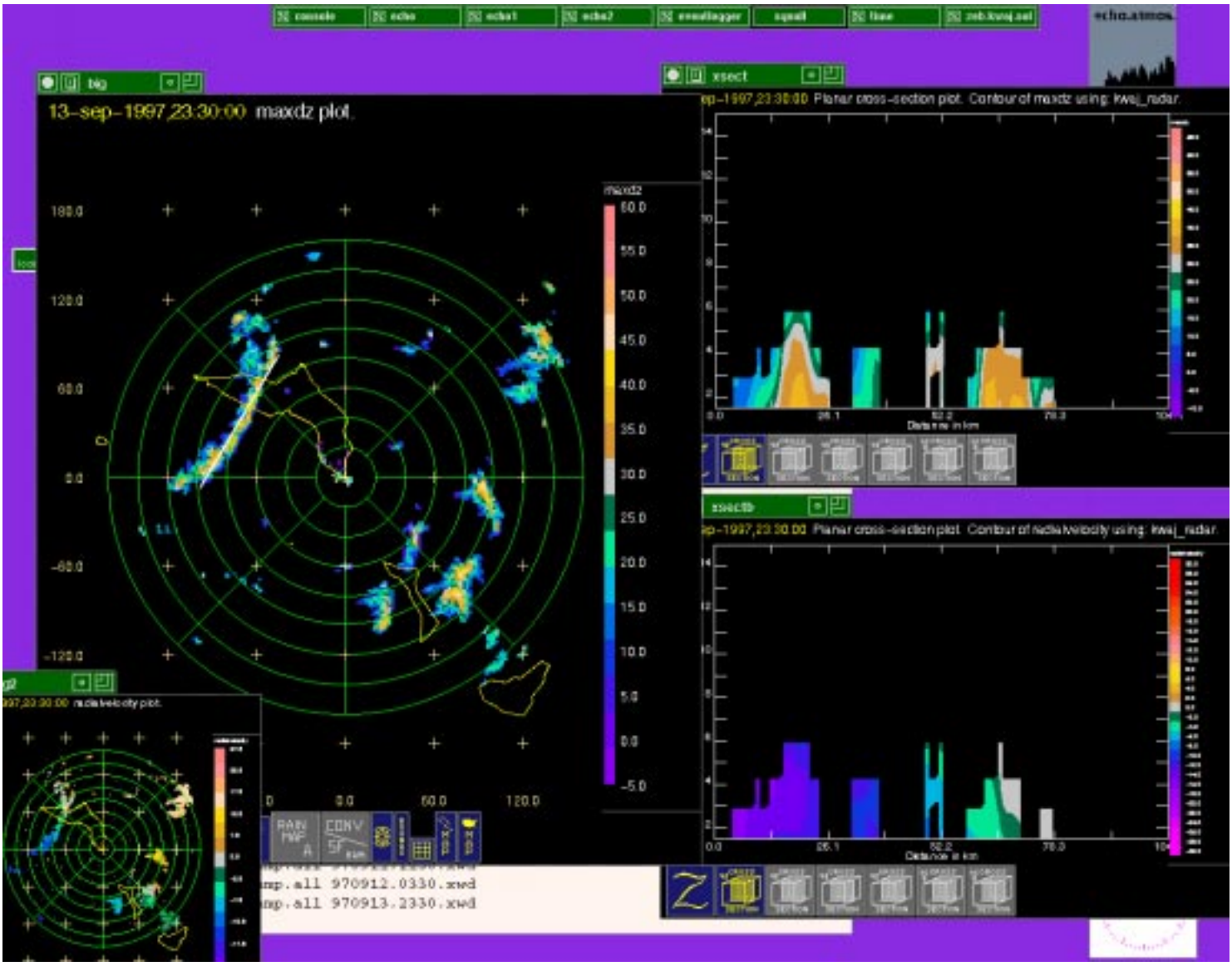

Figure 22. (continued)

(i)

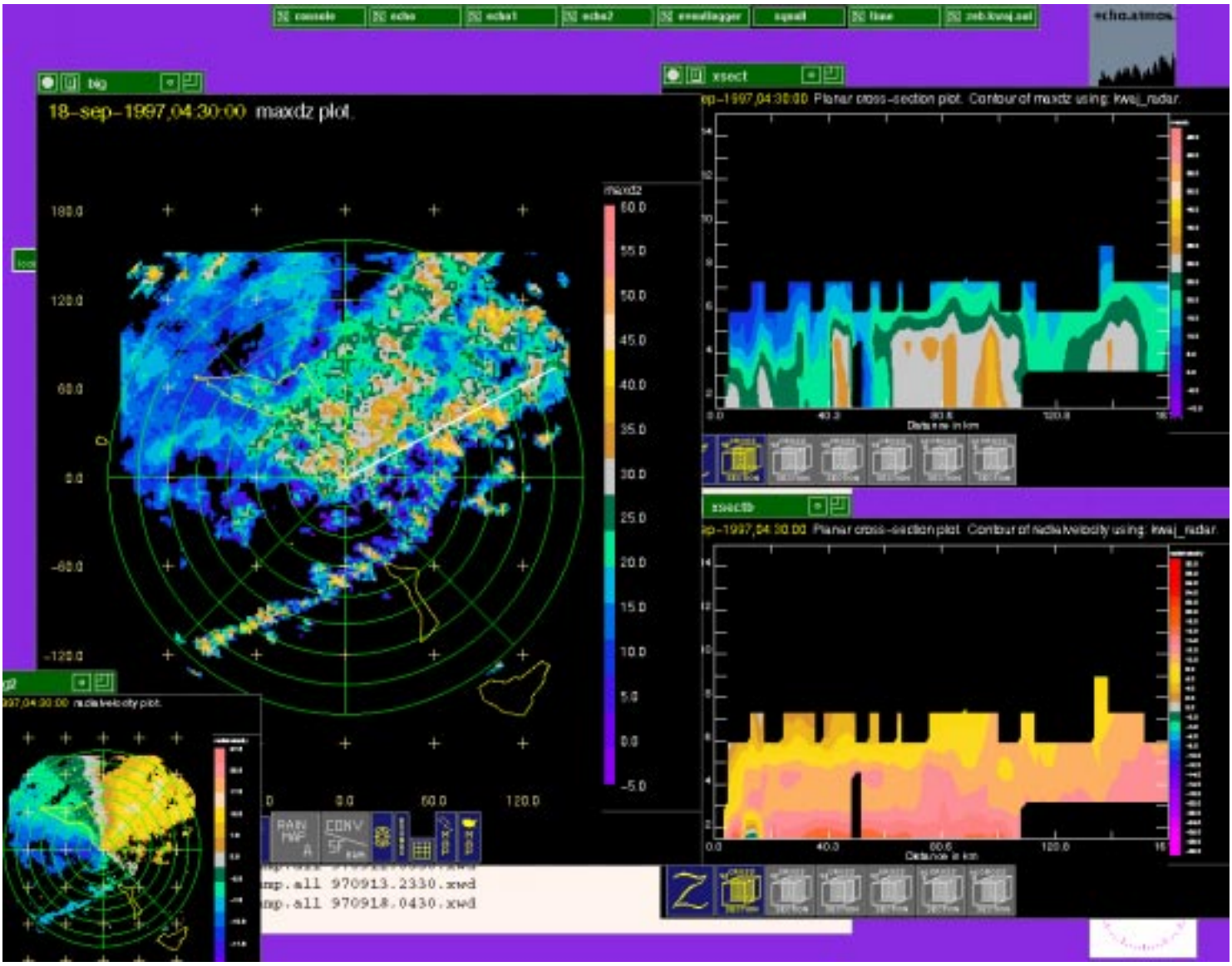

Figure 22. (continued)

(j)

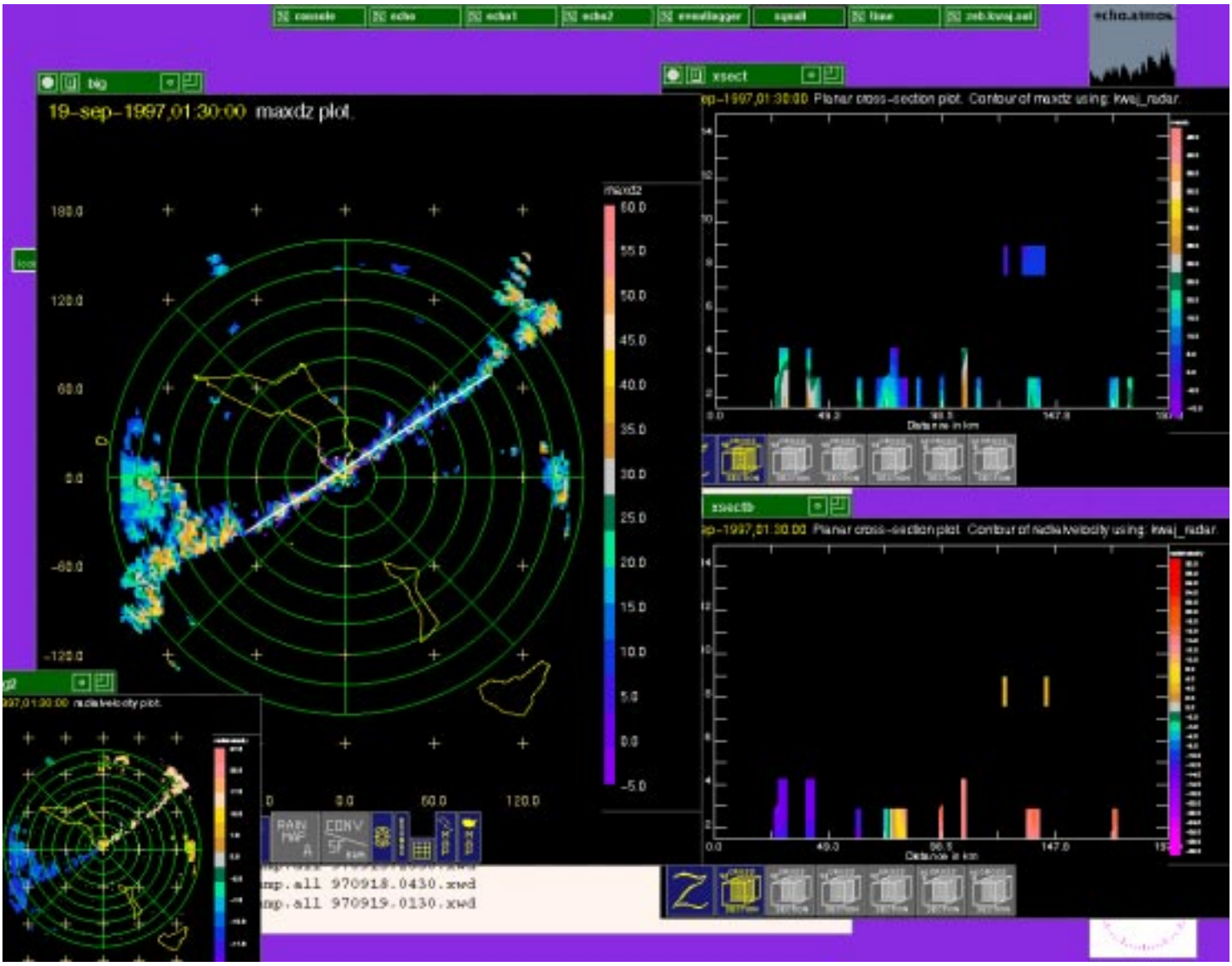

Figure 22. (continued)

(k)

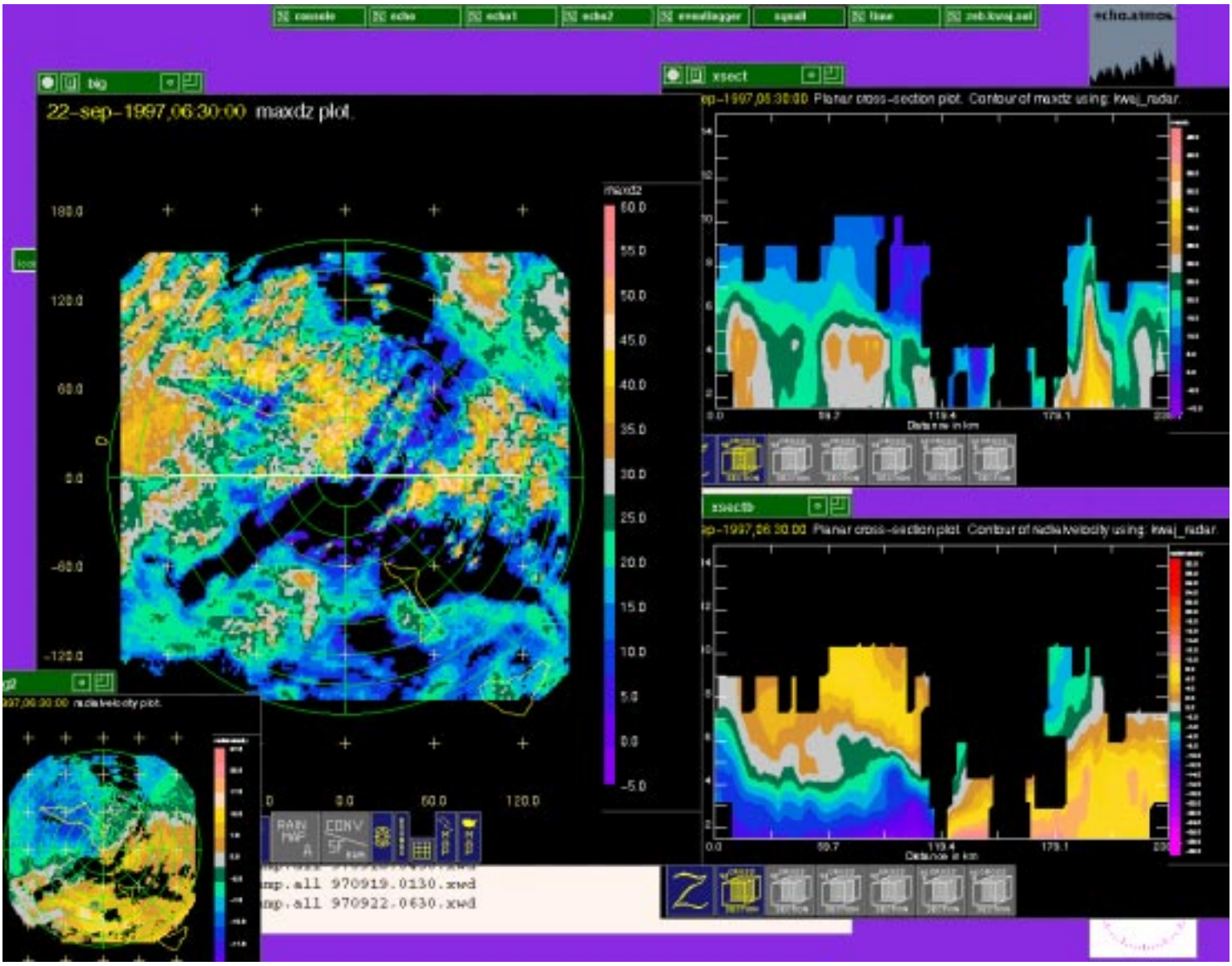

Figure 22. (continued)